Distinct stores and routing of water in the deep critical zone of a snow dominated volcanic catchment

Alissa White[1], Bryan Moravec[2], Jennifer McIntosh[1], Yaniv Olshansky[2], Ben Paras[1], R. Andres Sanchez[1], Ty P. A. Ferré [1], Thomas Meixner[1], Jon Chorover[2]

[1]Department of Hydrology and Atmospheric Sciences, University of Arizona, Tucson, 85721, USA

[2]Department of Soil, Water, and Environmental Sciences, University of Arizona, Tucson, 85721, USA

Correspondence to: Alissa White (alissawhite@email.arizona.edu)

Abstract. This study combines major ion and isotope chemistry, age tracers, fracture density characterizations, and physical hydrology measurements to understand how the structure of the critical zone (CZ) influences its function, including water routing, storage, mean water residence times, and hydrologic response. In a high elevation rhyolitic tuff catchment in the Jemez River Basin Critical Zone Observatory (JRB-CZO) within the Valles Caldera National Preserve of northern New Mexico, a periodic precipitation pattern creates different hydrologic flow regimes during spring snowmelt, summer monsoon rain, and fall storms. Hydrometric, geochemical, and isotopic analyses of surface water and groundwater from distinct stores, most notably shallow groundwater that is likely a perched aquifer in consolidated collapse breccia and deeper groundwater in a fractured tuff aquifer system, enabled us to untangle the interactions of these groundwater stores and their contribution to streamflow across one complete water year.

Despite seasonal differences in groundwater response due to water partitioning, major ion chemistry indicates that deep groundwater from the highly fractured site is more representative of groundwater contributing to streamflow across the entire water year. Additionally, comparison of streamflow and groundwater hydrographs indicates hydraulic connection between the fractured welded tuff aquifer system and streamflow while the shallow aquifer within the collapse breccia deposit does not show this same connection. Furthermore, analysis of age tracers and oxygen ($\delta^{18}O$) and stable hydrogen ($\delta^{2}H$) isotopes of water indicates that groundwater is a mix of modern and older waters recharged from snowmelt and downhole neutron probe surveys suggest that water moves through the vadose zone both as vertical infiltration and subsurface lateral flow, depending on lithology. We find that in complex geologic terrain like that of the JRB-CZO, differences in CZ architecture of two hillslopes within a headwater catchment control water stores and routing through the subsurface and suggest that shallow groundwater does not contribute significantly to streams while deep fractured aquifer systems contribute most to streamflow.

1 Introduction

Understanding the interconnections of groundwater and surface water is fundamental to water resource management as groundwater and surface water should be considered a single resource (Winter, 1998); however, their interactions in different hydrogeologic settings are varied and complex (Winter, 1999). Discerning stream water sources and groundwater dynamics are even more important in the context of changing climate, especially in the semiarid, mountainous environment of the western United States where warming trends are expected to threaten water supply (Barnett et al., 2005). Furthermore, identifying compartmentalized groundwater stores is necessary to sufficiently account for all components of the water balance (McDonnell, 2017). Therefore, characterizing localized water stores and the hydrologic connection of those aquifers to streams in mountainous environments that act as water towers (Viviroli et al., 2007) has important implications for water resource availability of large population centers downstream.

The influence of the hydrogeologic environment (i.e. geology, topography, and climate) on the groundwater flow system of a given geographic region has long been accepted as the theoretical framework used to conceptualize groundwater flow. Building on Toth’s (1970) conceptual model and the understanding that one part of the framework informs our knowledge of the other, several studies have focused on topography (Beven and Kirkby, 1979; Woods et al., 1997; Hutchinson and Moore, 2000; Kirchner et al., 2001; McGuire et al., 2005) and rock type (Farvolden, 1963; Freeze, 1972; Kelson and Wells, 1989; Mwakalila et al., 2002) as controls of groundwater flow systems. However, subsurface heterogeneities, which can be abundant and are challenging to identify, can give rise to complex, localized groundwater stores, whose contribution to streamflow can be very difficult to discern. There is still much to learn about the extent to which structural heterogeneities exist and how, specifically, they control groundwater storage, routing, and contributions to streamflow. For instance, evidence of perched aquifers transmitting shallow subsurface flow has been shown across variable rock types (Salve et al., 2012; Kim et al., 2014; Brantley et al., 2017; Kim et al., 2017; McIntosh et al., 2017). Furthermore, Brooks et al. (2015) highlighted the need to understand the influence of subsurface structure on water routing and residence time as they concluded that surface water, across several catchments and flow regimes, substantially interacted with or spent time within various soil and groundwater reservoirs. In fact, the lack of subsurface characterization in high elevation groundwater systems often forces hydrologic modeling studies to focus solely on shallow groundwater systems and make the generalizing assumption that hydraulic conductivity decreases with depth and deep fractured aquifers support little flow (Manning and Caine, 2007; Welch and Allen, 2014; Markovich et al., Accepted).

Heavily instrumented and intensively studied sites, such as Critical Zone Observatories (CZOs), which are part of a network of field-based laboratories arrayed across a variety of rock types, land uses, elevations and climates (Anderson et al., 2008), are ideal locations to examine the interplay between subsurface structure and function. Moreover, recent focus on characterizing the deep subsurface structure or architecture is beginning to elicit a deeper understanding of the role of weathering, lithology, and hydrology in overall critical zone (CZ) function and landscape evolution (Riebe et al. 2017). The CZ is the near-surface terrestrial layer of the Earth that spans from the tops of trees down to unweathered bedrock where water, rock, air, and life meet and interact (Brantley et al., 2006, 2007; Anderson et al., 2007; Chorover et al., 2007; Kusel et al., 2016). Herein, we use the term subsurface structure or architecture to refer to physical properties of the subsurface such as lithology, fracture density, and location and extent of geologic heterogeneities that may impact movement of water through the subsurface. Understanding the coupling between CZ architecture, developed over geologic time scales, and CZ function on short event time scales is a primary goal of CZ science (Chorover et al., 2011; Brooks et al., 2015). In particular, there is limited knowledge about the structure of the deep CZ and its direct influence on water storage (Holbrook et al., 2014; Dralle et al., 2018) and routing, mean residence times (McGuire et al., 2005), and streamflow sources. Integrated studies that simultaneously examine both, CZ architecture and CZ hydrology, through hydrometric, geophysical, geochemical, and residence time analyses are needed to understand the distribution of groundwater stores, their connection to streamflow, and the underlying impact of CZ architecture on hydrologic response to climatic drivers.

A current focus of hydrology is identifying and quantifying groundwater stores (Holbrook et al., 2014; McDonnell, 2017, Rempe and Dietrich, 2018; Dralle et al., 2018; Bhanja et al., 2018) and geophysics is an important tool for examining CZ architecture and its influence on water storage and movement. For example, McGuffy (2017) used seismic refraction surveys to estimate porosity and found that initial porosity plays a significant role in bedrock weathering in granitic and rhyolitic tuff CZs. Flinchum et al. (2018) took those porosity calculations a step further in using geophysics to estimate the water holding capacity of another granitic CZ; however, both studies noted the strong influence of, and uncertainty associated with degree of saturation of the media. Rempe and Dietrich (2018) used downhole surveys with a neutron probe to estimate rock moisture in the CZ and Dralle et al. (2018) used geophysics-based storage estimates from Rempe (2016) and Rempe and Dietrich (2018) to suggest differences in direct and indirect storage within the CZ from a coupled mass balance and storage-discharge function. The complexity of these estimates and their interactions highlights the need to couple geophysical approaches with subsurface interrogation, such as drilling and field characterization of hydraulic properties, to resolve this complexity, particularly in fractured heterogeneous environments.

In a headwater catchment and nested zero order basin (ZOB) within the complex volcanic Jemez River Basin Critical Zone Observatory (JRB-CZO), a considerable amount of research has been done to characterize the hydrology of the system. For instance, previous studies have explored energy limitations and topographic controls on hydrologic partitioning and water transit times (Zapata-Rios et al., 2015a, 2015b). Other studies used carbon pool and rare earth elements and ytrrium (REY) as biogeochemical tracers of streamflow generation (Perdrial et al., 2014; Vazquez-Ortega et al., 2015, 2016) and estimated groundwater contributions using end member mixing analyses (Liu et al., 2008a, 2008b). The most recent JRB-CZO studies explored concentration-discharge relationships to study seasonal shifts of hydrologic flow paths (McIntosh et al., 2017) and identify the hydrochemical processes governing the transport behavior of five distinct groups of solutes (Olshansky et al., 2018). Furthermore, studies agree that there is little overland flow contribution to streamflow in headwater catchments (Liu et al., 2008b; Perdrial et al., 2014; Zapata-Rios et al., 2015a) and subsurface flow is the primary contributor to streamflow (Liu et al., 2008a, 2008b; Perdrial et al., 2014; Vazquez-Ortega et al., 2015; Zapata-Rios et al., 2015a; McIntosh et al., 2017; Olshansky et al., 2018).

Studies spanning several water years have shown that spring snowmelt and summer monsoons induce different surface water flow regimes. More specifically, groundwater recharge appears to be restricted to winter snowmelt (McIntosh et al., 2017) and large evaporative fluxes diminish streamflow in summer months (Zapata-Rios et al., 2015a). However, seasonal groundwater changes have not been previously observed here and the interaction of different stores of water within the subsurface and the timing of their connection to streamflow are not understood. This gap motivated the current study, which sought to relate groundwater response, geochemistry, and age tracers across a full water year to the characterization of subsurface structure, mineralogy, and hydraulic properties. We hypothesized that there will be a more dramatic hydrologic response of shallow groundwater to spring snowmelt and a more gradual, small change after summer monsoon events. This study also aimed to elucidate how multiple groundwater stores within the CZ contribute to streamflow during different seasonal hydrologic flow regimes.

Most upland catchment studies to date have used springs as proxies for groundwater in the JRB-CZO; however, recent work by Frisbee et al. (2013) showed that while groundwater is a significant component of most springs, no springs are consistently composed entirely of groundwater and may also include soil water, unsaturated flow, and precipitation. With the recent drilling of a set of nested monitoring wells in a headwater catchment at the JRB-CZO (Figure 1B), we can now directly access groundwater from several depths within the CZ (Figure 2). This enabled the geochemical and isotopic analysis of groundwater and surface water from the JRB-CZO to answer the following research questions:

1) What is the seasonal hydrologic response of groundwater as a function of depth below ground surface in two hillslopes with contrasting lithology and CZ architecture?

2) How does CZ architecture, such as fracture density, lithology, and subsurface heterogeneities, influence water routing, mean residence times, and the seasonal contribution of distinct groundwater stores to streams?

To address these questions, we integrated several types of analyses including hydrometric, geophysical, geochemical, isotopic, and residence time tracers to examine the hydrologic response of ground and surface water and understand the connection between distinct groundwater stores and streamflow. We compared the timing of streamflow and groundwater response to climatic drivers, quantified temporal changes in subsurface water storage, defined distinct groundwater stores, inferred recharge processes from age tracers and oxygen ($\delta^{18}O$) and stable hydrogen ($\delta^{2}H$) isotopes of water, and examine how local flow processes relate to larger scale patterns.

2 Study Site and Methods

2.1 Site description

The Jemez River Basin Critical Zone Observatory (JRB-CZO) within the Valles Caldera National Preserve (VCNP) is situated in the Jemez Mountains in northern New Mexico northwest of Albuquerque (Figure 1A). This region is located in the transition zone between the snow dominated Rocky Mountains and the North American Monsoon (NAM) dominated deserts of the southwestern United States (Broxton et al., 2009). The JRB-CZO is in a montane, continental, sub-humid to semiarid climate characterized by a bimodal precipitation pattern (Zapata-Rios et al., 2015b). The VCNP is in a 21 km wide caldera that formed approximately 1.25 Myr (Bailey et al., 1969; Self et al., 1986). Ongoing volcanic activity as recent as 40 kyr caused the emplacement of several resurgent domes throughout the caldera (Wolff et al., 2011) of which Redondo Peak (3,432 meters above sea level, masl) is the largest. The JRB-CZO comprises several headwater catchments that drain different aspects of Redondo Peak. The geology of Redondo Peak is characterized by several faults and is dominated by Pleistocene Bandelier Tuff, rhyolite, and andesitic rocks (Broxton et al., 2009; Vazquez-Ortega et al., 2015) that were intermixed by collapse breccias in some locations (Hulen and Nielson, 1991), which created highly heterogeneous and complex geology (Figure 1B).

La Jara catchment and the Mixed Conifer Zero Order Basin (referred to as ZOB from here on), which is nested within the headwaters of La Jara, drain the eastern side of Redondo Peak (Figure 1B). La Jara catchment ranges in elevation from 2,702 to 3,429 masl with a mean slope of 15.7^{o} and drains an area of 2.66 km^2 (Perdrial et al., 2014). The ZOB consists of SE- and SW- facing slopes that are separated by a convergent zone and drains 0.15 km^2 (Vazquez-Ortega et al., 2016). The convergent zone of the ZOB, just above the ZOB flume, is characterized by boggy land in which standing water is present during the wettest parts of the year. Further evidence of near surface saturation in this area is the presence of marshy plants in standing water areas (e.g. broad-leaf cattails [*Typha latifolia*], rocky mountain irises [*Iris missouriensis*] and skunk cabbage [*Veratrum californicum*]), which contrast with those in the surrounding upland area of the ZOB (mostly bunch grasses [e.g. *Deschampsia*, *Festuca*, *Koeleria*, *Muhlenbergia*, and *Poa*] and aspen [*Populus tremuloides*] regrowth following a wildfire in 2013). Surface water from the ZOB flows through a Parshall flume before exiting the ZOB and then drains into La Jara creek.

Daily average precipitation and daily average temperatures were recorded at the Redondo Peak Weather Station (35.8839° N, 106.5536° W, 3231 m above sea level) maintained by the Desert Research Institute's Weather Regional Climate Center. Snow water equivalent (SWE) values were measured at the nearby Quemazon SNOTEL site (35.9167° N, 106.4000° W) located at a similar site elevation (2896 masl) in the Santa Fe National Forest about 5 km east of Redondo Peak. Cumulative precipitation depths are summed over one water year (from October 1 to September 30 of the next year).

2.2 Groundwater well completions Nested groundwater monitoring wells were drilled to total depths ranging from 6.7 to 47.2 meters below ground surface (mbgs) at each of three locations within the ZOB in June 2016 (Figure 1B and Figure 2). At each location, wells are separated laterally by no more than 2 m from the next well so that the well casings stand in a line. A LiBr tracer was mixed with fluids injected during the drilling and well development process. Br^- concentrations were measured in initial samples to ensure that drilling fluids were flushed from monitoring wells prior to analysis of groundwater samples. All screened sections of the well casing have 0.051 cm slotted intervals. All wells were drilled to depth with a diamond impregnated TT coring drill bit at an HQ3 diameter (9.6 cm annulus diameter; Supplemental Table 1). The annuli of all wells were packed with 8-12 CSS sand surrounding screened intervals and the sand packs were sealed with hydrated bentonite pellets.

Well 2D is situated above the deeper site 2 wells with approximately 20 m separation between the base of well 2D and the maximum water table of the next deepest well (well 2C) with a hydraulic head gradient between wells 2D and 2C slightly greater than unit gradient at 1.1 m. Without a fully screened well between the depths of 2D and 2C (Supplemental Table 1), we do not have direct evidence of an unsaturated zone between those wells and we did not measure saturation of cores collected during drilling because of the use of drilling fluids. However, cores collected during drilling provide evidence of redoximorphic features between the two wells that suggest the shallow well 2D is likely a perched aquifer.

2.3 Water Quality and Age Tracers

Differences in well casing diameter (Supplemental Table 4), depth of water column, sampling frequency, and seasonal site accessibility necessitated different sampling collection among wells. Groundwater samples were collected from site 1 wells (2.54 cm diameter casing) using a Waterra inertial pump (Waterra USA Inc., Peshatin, WA, USA). Groundwater samples from site 2 wells (5.08 cm diameter casing) were collected with a Geotech SS Geosub Pump (Geotech Environmental Equipment, Inc., Denver, CO, USA) except during times when snow accumulated leaving the site inaccessible by vehicle during which times samples were collected with a 42.1 mm stainless-steel bailer (Geotech Environmental Equipment, Inc., Denver, CO, USA). Approximately three borehole volumes were discarded before collecting samples from each well to ensure that formation water was retrieved. Surface water samples of La Jara and ZOB stream water were collected at flume sites as grab samples.

Groundwater and surface water samples were collected in acid washed polypropylene bottles (for cation analysis) and DI-washed, combusted amber glass bottles (for carbon content and $\delta^{18}O$ and $\delta^{2}H$ analysis). Bottles were triple rinsed with sample water prior to sample collection and samples were kept cold until promptly filtered at the University of Arizona. Sample splits for cations and trace elements were filtered through 0.45 μm nylon filters and acidified with trace metal grade nitric acid while all other splits were filtered through 0.7 μm glass fiber filters. Surface water samples were collected biweekly during dry seasons and twice daily at highest and lowest daily discharge using an automatic sampler (Teledyne, ISCO, NE, USA) during spring 2017 snowmelt. Groundwater samples were collected from all wells producing water on a biweekly basis during dry seasons and daily from the shallowest well (Well 2D; total depth 6.7 mbgs) during spring snowmelt using an autosampler (Teledyne ISCO, NE, USA).

All water samples were analyzed for cations, dissolved inorganic carbon (DIC), and $\delta^{18}O$ and $\delta^{2}H$. Cations were measured by inductively coupled plasma mass spectrometry (ICP-MS) at the University of Arizona Laboratory for Emerging Contaminants (ALEC). Dissolved inorganic carbon was measured with a Shimadzu TOC-VCSH carbon analyzer in ALEC. $\delta^{18}O$ and $\delta^{2}H$were measured with a DLT-100 Laser Spectrometer at the University of Arizona. Analytical precision (1σ) for all samples was 0.4 permil for $\delta^{2}H$ and 0.1 permil for $\delta^{18}O$. Stable isotope data from several previous studies at the JRB-CZO and surrounding locations were also incorporated (Vuataz and Goff, 1986; Longmire et al., 2007; Gustafson, 2008; Broxton et al., 2009; Zapata-Rios et al., 2015b).

Tritium analysis was completed at the University of Arizona Environmental Isotope Laboratory on select groundwater and surface water samples filtered through 0.45 μm nylon filters. Mean residence time (t) was calculated using the two most common lumped parameter models, the piston flow and exponential models, according to Eq. 1 and 2, respectively (Zuber and Maloszewski, 2000; Manga, 2001; Suckow, 2014; Zapata-Rios et al., 2015b)

$$C = C_0 e^{-\lambda t} \qquad \text{Piston Flow Model} \qquad (1)$$

$$C = \frac{C_0}{1+\lambda t} \qquad \text{Exponential Model} \qquad (2)$$

where C is the measured tritium concentration (reported as tritium units, TU) in groundwater, C_0 is the measured TU in local precipitation, and λ is the tritium decay constant (5.576×10^{-2} year^{-1}) based on a tritium half-life of 12.43 yr. Tritium analysis of precipitation in Albuquerque, NM (70 km from the study site) was measured monthly from 1962 to 2005 and are available as part of the Global Network of Isotopes in Precipitation (GNIP) through their Water Isotope System for data analysis, visualization, and Electronic Retrieval (WISER) database. Eastoe et al. (2012) found that volume weighted mean (VWM) tritium concentrations in Albuquerque precipitation have remained stable since the early 1990s and are similar to local prebomb atmospheric tritium concentrations. Zapata-Rios et al. (2015b) used SWE data from the previously described Quemazon station to calculate a VWM of background tritium (8.6 TU from 1992 to 2005) that is used as C_0 in mean residence time calculations herein. The uncertainty of age calculations was computed according to Eq. 3 following Bevington and Robinson (1992), Scanlon (2000), and Zapata-Rios et al. (2015b)

$$\sigma_t = \left[\left(\frac{dt}{dc_0}\right)^2 {\sigma_{c_0}}^2 + \left(\frac{dt}{dc}\right)^2 {\sigma_c}^2\right]^{0.5} \qquad \text{Age Uncertainty} \qquad (3)$$

where σ_t is the uncertainty of the age calculation, σ_{C_0} is the uncertainty of the background tritium concentration calculated as the mean of all lab reported error of tritium measurements reported for Albuquerque, and σ_C is the uncertainty (lab reported error) in the measurement of tritium in samples in this study. It is important to note that the calculated residence times are biased towards shorter times because tritium in groundwater with a residence time greater than 25 years would have entered the groundwater system before the time frame of constant tritium levels over which the VWM tritium input was calculated. Therefore, the actual tritium input was likely higher than the VWM tritium input used in residence time calculations and calculated residence times are likely underestimates.

Groundwater samples from wells 2D and 2C were collected with Hydrasleeve™ (GeoInsight, Las Cruces, NM, USA) passive collector bags in February 2018 for ^{14}C analysis. Self-sealing bags were deployed in the wells and left to equilibrate for 24 h before sample retrieval. Radiocarbon analysis was completed at the University of Arizona Accelerator Mass Spectrometry (AMS) Laboratory on DIC in groundwater samples. Measured ^{14}C activities are expressed as percent modern Carbon (pmC) that were calculated as weighted averages of combined machine runs to reduce overall error and $\delta^{13}C_{DIC}$ measured values are expressed as permil.

Uncorrected radiocarbon ages were computed following Eq. 4 for radioactive decay using a ^{14}C half-life of 5730 years and an initial ^{14}C activity (A_0) of 100 pmC, according to data from the neighboring Española Basin bound to the west by the Jemez Mountains (Manning, 2009). In order to calculate corrected radiocarbon ages, the $\delta^{13}C_{DIC}$ value of the recharge water (-16.13 ‰) was first calculated based on an assumed temperature of recharge of 9.6 ºC (the average temperature of soil water from the ZOB over the last year of consecutive measurements, 2011), pH of 7.51 (the average pH of soil water from the ZOB over the last year of consecutive measurements, 2011), and a $\delta^{13}C_{CO2}$ of ZOB vegetation of -24.7 ‰ (unpublished data from Tjasa Kanduc) using equilibrium constants of the carbonate system (Drever, 1997), alpha values between $CO_{2(g)}$ and $CO_{2(aq)}$ according to Vogel et al. (1970), and alpha values between HCO_3^- and $CO_{2(aq)}$ and between HCO_3^- and CO_3^{2-} according to Mook et al. (1974).

Corrected ages were calculated using the $\delta^{13}C$ mixing model of equations 5 and 6 following Pearson (1965), Pearson and Hanshaw (1970), and Clark and Fritz (1997) using an assumed $\delta^{13}C_{DIC}$ of calcite of 0 ‰, a calculated value of $\delta^{13}C_{DIC}$ value of the recharge water, and A_0 of 100 pmC.

$$t = -\lambda \, ln(\frac{A_{sample}}{A_0}) \qquad \text{Uncorrected Age} \qquad (4)$$

$$q_{\partial 13\mathrm{C}} = \frac{\partial^{13}C_{measured} - \partial^{13}C_{carbonate}}{\partial^{13}C_{recharge} - \partial^{13}C_{carbonate}} \qquad \delta^{13}\text{C Fraction from Atmospheric Carbon} \qquad (5)$$

$$t = -\lambda \, ln(\frac{A_{sample}}{q_{\partial 13\mathrm{C}} * A_0}) \qquad \text{Corrected Age} \qquad (6)$$

2.4 Streamflow and Groundwater Depths

Streamflow measurements were recorded at 15 min intervals from pressure transducers inside the stilling well of a Parshall flume at the base of the ZOB at 2996 masl and La Jara catchment at 2739 masl (flume locations shown in Figure 1B). Transducer data were calibrated by depth measurements taken by hand at the time of each sampling event.

All monitoring wells were installed with vibrating wire piezometers (VWP) during the drilling campaign to provide nearly continuous (15 min) measurements of hydraulic head in each well (Supplemental Figure 1). In this study, time series of groundwater depths are only shown from two wells (Well 1A and Well 2D) with continuous monitoring via VWPs. Electronic sounder measurements of depth to water were taken before every groundwater sampling event, converted into depth of water column above VWP, and used to calibrate VWP and transducer measurements.

2.5 Saturated hydraulic conductivity estimates

Nearly continuous monitoring of hydraulic head in groundwater wells enabled individual sampling events to be treated as rising-head bail-down slug tests (Butler, 2015). Aqtesolv software (Duffield, 2007) was used to curve fit aquifer response (VWP measurements of depth of water converted into normalized change in water table height against the logarithm of elapsed time) using the Kansas Geological Survey (KGS) model (Hyder et al., 1994) for three sampling events in wells 1A and 2D to estimate saturated hydraulic conductivity (K_{sat}) values using the Aqtesolv Automatic Estimation procedure. Early time recovery (first 15 min after disturbance) was missed between time intervals so the largest normalized head displacement is approximately 0.8 (m m^{-1}). Loss of early time data (beginning H/H_0 of 0.8) from Pratt 4-2 slug test data (Butler, 1998; data available from http://www.aqtesolv.com/examples/uncslug1.htm) produced 1.07% error in K_{sat} values. Slug test analysis assumed isotropy.

2.6 Volumetric water content in soil pedons

Decagon EC-5 soil moisture sensors measured volumetric water content (VWC) in 6 instrumented soil pedons within the ZOB (Figure 1) ranging from depths of 9.5 to 65 cm below ground surface (cm bgs). Decagon soil moisture sensors measure the dielectric constant of soil, which is a sensitive measure of water content because of the much higher dielectric constant of water compared to that of soil and air. Dielectric constant measurements in mV are converted to VWC in m^3 m^{-3} according to the Decagon EC-5 factory calibration equation. VWC was measured at multiple depths in four of the six pedons. VWC was recorded every 10 min.

2.7 Downhole neutron probe surveys

Water content profiles with depth were determined from neutron probe (Model 503DR, Campbell Pacific Nuclear, Concord, CA, USA) surveys within the vadose zone in the top 18.3 mbgs in wells 2B and 2C and the total depth of well 3B (12.9 mbgs) over four different events. Raw neutron counts were recorded by the detector using a 32 second interval. Measurements were recorded every 0.3 m and a minimum of three readings were taken at each depth. Standard counts were measured in an acrylic sleeve before and after measurements of each well and were used to correct for radioactive decay of the Am-241:Be source. Wet and dry calibrations were completed by measuring neutron counts within a 55-gallon drum filled with Viton sand surrounding a PVC casing (same material as well casing). The calibration between neutron counts and water content is generally linear up to water contents of 0.4 (Rempe, 2016), which is greater than the maximum water contents measured here; however, neutron probe counts are sensitive to changes in bulk density and variable solid phase chemical composition (Gardner et al., 2000; Rempe, 2016). Because of the highly heterogeneous geology and mineralogy in the JRB-CZO ZOB (Moravec et al., 2018), one calibration material (Viton sand) was used for all wells and all depths, which limits the interpretation of neutron probe surveys to comparison over time at the same site.

2.8 Fracture Traces and Density Estimates

Downhole images captured with an optical televiewer at site 1 and 2 wells were used to identify fracture traces and calculate fracture density using the Fracture Pattern Quantification (FracPaQ) MATLAB™ toolbox available as open source code via Mathworks™ FileExchange (Healy et al., 2017). Near surface borehole instability required steel casing from the surface down to approximately 15 mbgs, which necessitated that downhole images, and thus fracture density characterization, started at approximately 15 mbgs. Because of the variable mineralogy and corresponding color transitions in the boreholes, it was necessary to trace fractures seen in optical televiewer images of wells 1A and 2A onto a new layer in Adobe Illustrator™. The scalable vector graphics (.SVG) file of the polyline fracture traces without the underlying downhole image was used as the input file for FracPaQ (Healy et al., 2017), which extracted the x and y fracture-trace coordinates from the file. Fracture density is defined as the number of fractures per unit area and has the units of m^{-2} (Dershowitz and Herda, 1992). FracPaQ (Healy et al., 2017) calculates fracture density from the fracture segment network as $m/2\pi r^2$ according to Mauldon et al. (2001) where m is the number of trace endpoints in circle of radius r by resampling the exposed traces using circular scan windows that eliminate orientation, censoring, and length biases.

3 Results

3.1 Temporal analysis of hydrographs and soil moisture

Temporal analysis of the climatic parameters (daily precipitation and temperature, Figure 3A, and snow water equivalent (SWE), Figure 3B) that drive streamflow response in ZOB and La Jara surface waters (Figure 3C and Figure 3D, respectively) and groundwater from the fractured tuff (Well 1A, Figure 3E) and shallow aquifers (Well 2D, Figure 3F) are used to examine seasonal hydrologic responses. Snow water equivalent peaked at 213 mm during WY 2017 while annual cumulative precipitation was 673.5 mm for water year 2017. The average temperatures during summer and winter months of WY 2017 were 13.4ºC and -4.2 ºC, respectively. As temperatures rose above freezing, the snowpack began to melt and SWE values dropped rapidly (Figure 3A and B). In response to snowmelt, daily averaged discharge of the ZOB flume peaked while La Jara streamflow peaked. Temperatures dropped below freezing again causing ZOB streamflow to freeze producing no measured discharge while La Jara streamflow reached a local minimum. During freezing temperatures, a second short-lived snowpack accumulated 18 mm of SWE. As temperatures increased above freezing again, maximum flows were reached in La Jara flume because streamflow remained high above baseflow conditions between snowmelt peaks and a local streamflow maximum was reached in ZOB flume. While streamflow peaks were greatest in response to spring snowmelt, there were also obvious, smaller peaks in ZOB and La Jara surface waters following summer monsoons and fall storms. Both snowmelt and rainfall events influenced La Jara creek and ZOB streamflow leading to increases above baseflow (Figure 3C and D, respectively). However, the major driver of streamflow and groundwater depth response was spring snowmelt.

The depth of water in wells 1A and 2D (Figure 3D and F, respectively) also responded to spring snowmelt, summer monsoons, and fall rainfall. Well 1A water depths peaked just two days after SWE values dropped to zero and on the same day that La Jara streamflow reached a local maximum. As temperatures froze again and a second snowpack developed, well 1A depth of water receded until 4/6/17 after which it quickly rose to a second local maximum on 4/11/17 four days before ZOB streamflow reached a second max and six days before La Jara streamflow reached its second peak. Well 1A water depths also peaked sharply on 10/2/17 in response to fall precipitation. Conversely, well 1A water depths reached one gradual peak during NAM season on 8/16/17, despite several smaller La Jara streamflow peaks in response to summer monsoon storms.

Water depths in well 2D (Figure 3F) did not have pronounced, sharp maxima and minima in response to snowmelt dynamics like those seen in surface waters and site 1 groundwater. Instead, water depths in well 2D continued rising, with slight changes in rate on 3/21/17 and 4/4/17, while temperatures dropped below freezing again and a second snowpack accumulated and melted before well 2D water depths peaked on 4/22/17. Well 2D water depths did not respond to summer monsoons and, instead, continuously decreased after their spring snowmelt peak until reaching a minimum after summer monsoons on 10/4/17. However, the well 2D water table gradually increased in response to fall storms until reaching peak water depths on 10/25/17. It appears that water slowly infiltrated into the shallow aquifer and recharged the near surface groundwater store.

Volumetric water content (VWC) in ZOB soils from six pedons ranging from 9.5 to 65 cm bgs also varied seasonally with generally higher VWC during spring snowmelt, lower VWC at the onset of NAM season, and intermediate VWC during fall storms (Figure 4). VWC changes across the water year at the shallowest depth in pedons 4 and 3, located in the western area of the ZOB nearest site 2 wells, were small (0.20 m^3 m^{-3} range in pedon 4 and 0.16 m^3 m^{-3} range in pedon 3), while VWC at greater depth in pedon 3 increased drastically and remained elevated during spring snowmelt and fall storms. Changes in VWC are likely most pronounced at depth due to subsurface lateral flow through more saturated, more conductive media, as suggested by previous studies in the JRB-CZO (Liu et al., 2008; McIntosh et al., 2017; Olshansky et al., 2018). Changes in VWC at pedons 5 and 2, located in the convergent zone of the ZOB nearest site 3 wells, were most pronounced during spring snowmelt. Again, increased VWC in pedon 2 persisted longer at depth than at the near surface. While located in the same tuff rock type as pedon 5 situated in the ZOB's convergent zone, soils in the eastern area of the ZOB near site 1 wells at pedons 6 and 1 were located upslope of the convergent zone and did not remain wet for extended periods, but rather increases in VWC of pedons 6 and 1 were flashy while decreased VWC during NAM season was sustained. Estimates of saturated hydraulic conductivity of wells 1A and 2D were computed to explore differences in hydrologic properties of the two groundwater reservoirs following three sampling events that served as bail-down slug out tests. Averaging K_{sat} from the three events produced a mean for well 2D of 7.22 x 10^{-3} m day^{-1} and 1.22 x 10^{-4} m day^{-1} for well 1A (Table 1), despite fracture density of deeper site 2 wells estimated to be approximately five times less than fracture density of site 1 wells (Figure 5). However, it is important to note that fracture density could not be calculated across the water table depths of well 2D or site 1 wells because of surface instability and presence of water inhibiting downhole televiewer images.

3.2 Neutron probe profiles

Soil moisture content in two site 2 boreholes (Wells 2B and 2C) and one site 3 borehole (Well 3B) were estimated from a neutron probe soil moisture gauge that was run downhole on four dates. Due to the textural shifts and complexity of mineral composition as a function of depth at each site and across sites (Moravec et al., 2018), water content estimates are used to qualitatively examine changes in water content with depth and over time within each respective borehole.

Profiles of water content with depth below ground surface in borehole 2B (Figure 6, left), reach a local maximum water content of approximately 0.32 cm^3 cm^{-3} at 1 mbgs during all events. At increased depth, the water content recedes to an overall minimum of 0.15 cm^3 cm^{-3} at 2.4 mbgs in the June, August, and February measurements while the October measurement recedes to only 0.23 cm^3 cm^{-3} at 1.8 mbgs before spiking to 0.36 cm^3 cm^{-3} at 2.4 mbgs and receding slightly to 0.35 cm^3 cm^{-3} at 4 mbgs below which depth changes in water content are consistent across all time series.

In borehole 2C (Figure 6, center), just 2 m away from borehole 2B, differences in water content profiles are also seen over time. In October, water content increases from the surface until reaching an overall maximum of 0.4 cm^3 cm^{-3} at 3.7 mbgs whereas profiles from the other three events peak at 0.29 cm^3 cm^{-3} at only 0.6 mbgs, recede to 0.08 cm^3 cm^{-3} at 1.2 mbgs and increase gradually to 0.12 cm^3 cm^{-3} at 3.4 mbgs and drastically jump up to a range of water content from 0.34 to 0.39 cm^3 cm^{-3} (July to Feb, respectively) at 4 mbgs. From 4 to 15.5 mbgs, the water content profiles for all events are relatively consistent between 0.28 cm^3 cm^{-3} and 0.30 cm^3 cm^{-3} (June and August identical, October 0.1 greater than summer profiles, and Feb 0.1 greater than October).

Finally, water content profiles with depth in borehole 3B (Figure 6, right) are nearly identical across all measurement events and show three peaks in water content of 0.36 cm^3 cm^{-3}, 0.33 cm^3 cm^{-3}, and 0.25 cm^3 cm^{-3} at 1.2, 8.5, and 11.6 mbgs, respectively.

3.3 Geochemistry

In a volcanic setting such as the Valles Caldera, silicate mineral weathering is the primary driver of stream water chemical fluxes (McIntosh et al., 2017) and larger concentrations of base cations have been found in waters with longer flow paths as mineral dissolution fluxes increase with increasing water transit times (Zapata-Rios et al., 2015b). Quantitative mineralogy of cores collected during the June 2016 drilling campaign in the ZOB (Moravec et al., 2018) found that quartz, potassium feldspar, plagioclase, volcanic glass, and smaller percentages of mica are the primary minerals ubiquitous in site 1 and 2 cores. Smectite, iron oxides, illite, and magnesite, as well as diagenetically altered minerals like Ca-zeolites (clinoptilolite and mordenite), are present in smaller percentages within the top 15 mbgs of site 1, along with some 2:1 clays from 15 to 17 mbgs and 20 to 26 mbgs. Ca-zeolites, smectite, illite, iron oxides, and trace talc and tremolite are also found throughout site 2 cores, as well as secondary minerals like calcite and illite in the top 15 mbgs. Greater percentages of 2:1 clays are also found throughout site 2 cores, especially from 12 to 16 mbgs and 22 to 30 mbgs. Previous analysis of saturation indices of ZOB groundwater found that well 2D shallow groundwater fluctuated between near equilibrium and over saturation with respect to calcite (Olshanksy et al., 2018), while previous work by Zapata-Rios et al. (2015b) found that springs across the JRB-CZO were undersaturated with respect to calcite, albite, and sanidine; therefore, interaction with those minerals is expected to influence groundwater and surface chemistry in the ZOB and La Jara catchment.

The primary groundwater cations from each monitoring well are Ca^{2+}, Na^{+}, and Mg^{2+} (Table 2); however, the percentages (in terms of μeq/L) of each cation differ between sites (Sites 1 and 2). Major ion concentrations also differ with depth between site 2 wells while site 1 groundwaters (Wells 1A and 1B) are geochemically similar to one another (Supplemental Figure 1). These differences in cation concentration are used in further analysis to distinguish streamflow sources.

Temporal analysis of major cation concentrations in groundwater and surface water over WY 2017 (Figure 7) again shows clear separation of groundwater concentrations between the two sites. Ca^{2+} and DIC concentrations are highest in the shallow aquifer (Well 2D), where calcite is known to be present, and all site 2 groundwater Ca^{2+} and DIC concentrations are considerably greater than surface and site 1 water year-round (Figure 7). Furthermore, Ca^{2+} and DIC concentrations are most variable in wells 2D and 2C, which change together in time, suggesting a connection between the two water stores. Finally, both Ca^{2+} and DIC concentrations of shallow groundwater increase simultaneously during spring snowmelt at the time that La Jara streamflow increases above baseflow, which is likely from calcite dissolution. In contrast, Ca^{2+} and DIC concentrations of La Jara surface waters do not change markedly as streamflow increases while Ca^{2+} and DIC concentrations of ZOB surface waters decrease slightly during this time. Mg^{2+} concentrations are greatest in the deepest well (Well 2A) and decrease with decreasing depth at site 2, are lower still in site 1 groundwater, and lowest in La Jara stream water (Table 2). Na^{+} concentrations of the shallow aquifer increase steadily at the onset of snowmelt while La Jara and ZOB surface water Na^{+} concentrations decrease slightly (Figure 7). As the site 1 water table slowly recedes following spring snowmelt, Na^{+} concentrations in well 1A increase likely because of the weathering of feldspars. Unfortunately, the lack of site 1 groundwater data during snowmelt makes it impossible to determine if the variability of site 1 groundwater chemistry resembles that of surface waters; however, surface water concentrations of major ions are generally closer in magnitude to those of site 1 groundwaters throughout the remainder of the water year.

Comparison of Ca^{2+}/Mg^{2+} molar ratios with Na^{+} concentrations (Figure 8A) and DIC concentrations (Figure 8B), which can differentiate between weathering of Ca^{2+} rich and Mg^{2+} rich silicate minerals, also show distinct groupings of groundwater between sites and depths. The Ca^{2+}/Mg^{2+} molar ratios of the shallow aquifer are greater than those of the deeper waters. The Ca^{2+}/Mg^{2+} molar ratios of surface waters overlap in space with those of deeper groundwater. The DIC concentrations clearly differentiate between sites 1 and 2 and the surface waters plot with similar DIC concentrations as site 1 groundwater, which indicates that deeper groundwater from site 1 is more representative of streamflow in La Jara catchment.

3.4 Age tracer analysis

Oxygen ($\delta^{18}O$) and stable hydrogen ($\delta^{2}H$) isotope values of groundwaters and surface waters are comparable to one another. In addition, $\delta^{18}O$ and $\delta^{2}H$ values of both groundwaters and surface waters are more similar to the lower isotope values of snow than to those of summer precipitation (Figure 9) indicating that snowmelt is the dominant source of recharge to groundwaters and surface waters in the ZOB and La Jara catchment. The majority of samples plot along the local meteoric water line (LMWL; from Broxton et al. (2009)), showing consistency in $\delta^{18}O$ and $\delta^{2}H$ values over time. However, several surface waters and a few samples of deep groundwater from site 1 wells and shallow groundwater from well 2D have higher $\delta^{18}O$ and $\delta^{2}H$ values that plot to the right of the LMWL, along an enrichment line with a slope of 3.4 (Figure 9).

Tritium was detected in groundwater from each sampled well, which indicates that there is a component of modern recharge to all groundwater stores (Manning, 2009). Tritium content from wells analyzed in June 2017 and February 2018 are within two standard errors of one another indicating little difference between the tritium content of groundwater stores between the summer dry season and the winter. The highest tritium content (4.4 TU in February 2018) and therefore shortest residence time waters (12 and 17 years according to piston flow and exponential models, respectively) are those of the shallow aquifer while the lowest tritium content (0.7 TU in February 2018) and longest residence times (45 and 202 years, according to piston flow and exponential models, respectively) are from wells 2B and 2C (Table 3). As expected, there is more tritium present in the shallowest groundwater compared to deeper waters from site 2 wells; however, the deepest site 2 groundwater from well 2A has more tritium than the shallower wells 2B and 2C. Differences in tritium content (Table 3) across similar depths from sites 1 and 2 (Figure 2) indicate the presence of separate groundwater stores of water within the ZOB.Radiocarbon age calculations were computed for shallow groundwater from well 2D and groundwater from well 2C beneath the shallow aquifer based on ^{14}C activity and $\delta^{13}C$ of DIC of the two wells. The ^{14}C activity of DIC from well 2D was 75.34 ± 0.19 pmC while the $\delta^{13}C_{DIC}$ was -13.1 ‰, which corresponds to a corrected radiocarbon age of 621 years. The ^{14}C activity of DIC from well 2C was 60.02 ± 0.17 pmC and the $\delta^{13}C_{DIC}$ was -12.4 ‰, which corresponds to a corrected radiocarbon age of 2050 years (Table 3). As expected, there is less modern ^{14}C-DIC in the deeper groundwater (Well 2C) indicating longer residence times at greater depth.

Discussion

This study seeks to understand the seasonal hydrologic response of groundwater as a function of depth below ground surface at sites 1 and 2 and to explore how CZ architecture influences water routing and seasonal groundwater contribution to streamflow in La Jara catchment. Distinct geochemical signatures of deep groundwater from a highly fractured aquifer system and shallow groundwater that is likely a perched aquifer in a collapsed breccia deposit used in combination with geochemical and hydraulic head time series of shallow and deep groundwater and surface water from the catchment outlet enable us to decipher the effect of the contrasting CZ architecture and lithology of sites 1 and 2 on streamflow generation. The following sections discuss the dynamics of seasonal hydrologic response, water routing, recharge and water residence times, major ion chemistry, and CZ architecture to investigate streamflow contributions over time.

4.1 Hydrologic response

Site 1 wells are situated in highly fractured welded tuff with maximum fracture density of approximately 5000 m^{-2}. This contrasts with highly weathered volcanic breccia in the top 15 mbgs at site 2 wells that corresponds with a caldera collapse breccia deposit overlying more consolidated, less fractured welded tuff with maximum fracture density of approximately 1000 m^{-2} at depth (Figure 5). We hypothesize that the differences in subsurface structure, presence of a confining layer, and greater fracture density of site 1 wells compared to site 2 wells (Figure 5) influences the different hydrologic response of the two sites (Figure 3). Well 1A responds rapidly to snowmelt, reaching its first peak on the same day as La Jara streamflow's first peak, and responds gradually to summer monsoon events (Figure 3E). Well 2D has a muted response to snowmelt with the first inflection point occurring on the same day as the first ZOB discharge peak while the first well 2D water table maximum occurs 45 days after the onset of snowmelt and does not respond to summer monsoon events at all (Figure 3F).

Mean K_{sat} values from both wells (Table 1) are lower than K_{sat} estimates of the same Tshirege member of Bandelier Tuff from nearby Los Alamos National Lab that range from 7.6 x 10^{-2} to 1.12 m day^{-1} (Rogers and Gallaher, 1995; Smyth and Sharp, 2006) and 9.3 x 10^{-1} to 1.6 x 10^{1} m day^{-1} (Kearl et al., 1990; Smyth and Sharp, 2006). This may be, in part, because slug tests provide localized estimates of the hydraulic conductivity directly surrounding the screened interval of the well in contrast to pumping tests that provide larger scale volumetric averages of hydraulic properties. Butler (2015) notes that hydraulic conductivity estimates from slug tests should be viewed as lower bounds of the conductivity in the vicinity of the well. Furthermore, the degree of welding and presence of alteration may account for the discrepancies in conductivity estimates as Rogers and Gallaher (1995) noted that the degree of welding of the Bandelier Tuff was greatest closer to the Valles Caldera, the tuff's volcanic source and site of this study.

Surprisingly, the mean K_{sat} of the shallow aquifer (Well 2D) is more than one order of magnitude greater than that of the deep well 1A (7.22 x 10^{-3} m day^{-1} and 1.22 x 10^{-4} m day^{-1}, respectively, Table 1). Many more fractures are present at site 1 relative to site 2 (Figure 5A), which generates a fracture density approximately 5 times greater at site 1 wells than site 2 wells (Figure 5B). Unfortunately, it is not possible to directly compare the fracture density across the screened intervals from which hydraulic conductivity estimates were made because downhole images could not be captured within either well at those depths, but we expect that the general trend of dense fractures at site 1 and few fractures at site 2 would persist. The lower mean K_{sat} of well 1A could suggest that fractures may be backfilled by mineral precipitates and weathering rinds decreasing the ability of fractures to act as preferential flowpaths. It is noteworthy, however, that such a mechanism is not clearly supported by the downhole images or core samples; these images and cores do not show obvious evidence of backfilled fractures.

Despite unexpected K_{sat} differences between the two wells, the very similar shape and timing of well 1A's hydrograph compared to those of La Jara stream and ZOB surface water (Figure 3) is a function of pressure propagation and indicates hydraulic connection between the fractured aquifer system and streamflow (Sophocleous, 1991a; Welch et al., 2013). The rapid pressure pulse transfer between site 1 groundwater and the stream suggests that the fractured welded tuff aquifer system has low specific storage and high transmissivity. Worthington (2015) noted much more rapid changes in head in low storage fractured bedrock aquifers compared to granular aquifers and Sophocleous (1991a) found that the hydraulic diffusivity is the major control of the extent and speed of pressure pulse propagation.

The rapid response of the welded tuff aquifer system (Well 1A, Figure 3E) contrasts with the muted response of the shallow aquifer (Well 2D, Figure 3F), which does not show evidence of pressure pulse propagation between shallow groundwater and the ZOB and La Jara surface waters. The slower response of groundwater levels in well 2D suggests that the shallow aquifer is not directly hydraulically connected to the stream likely because it appears to be separated from deeper groundwater by a low permeability confining layer and the significantly lower fracture density of site 2 wells (Figure 5). The comparison of site 1 and 2 groundwater hydrographs to surface water hydrographs bears a striking resemblance to the juxtaposition of stream-flood wave propagation in monitoring wells drilled into buried river channels (similar to well 1A) and the absence of pressure pulses in monitoring wells not associated with buried channels (similar to well 2D) seen in the Great Bend alluvial aquifer in Kansas (Sophocleous, 1991a). Furthermore, the cubic shape of the rising water table in the shallow aquifer identified by the slow initial rise of groundwater levels followed by an inflection point and subsequent rapid rise in well 2D groundwater levels (Figure 3F) is indicative of groundwater recharge (Sophocleous, 1988, 1991a, 1991b). Further analysis of the rates of increase before and after the well 2D hydrograph inflection point can be found in Olshansky et al. (2018).

Hydrologic response to incoming precipitation exhibits strong dependence on season, as indicated by differences following spring snowmelt, summer monsoons, and fall precipitation. Specifically, well 1A groundwater responds rapidly to spring snowmelt and fall precipitation, in contrast to the welded tuff aquifer's response to summer monsoon rain that is smaller and much more gradual, suggesting that spring snowmelt and fall precipitation induce a different hydrologic flow regime than that of summer monsoons (Figure 3E). Different hydrologic flow regimes across seasons also exist in the shallow aquifer (Well 2D). While all changes in the shallow water table are gradual, spring snowmelt and fall precipitation produce water table peaks in late April and October while the shallowwater table steadily decreased during summer monsoons indicating no water table changes induced by summer storms (Figure 3F).

The less pronounced hydrologic response to summer monsoons, compared to snowmelt and fall rain, in shallow groundwater of site 2 and deeper groundwater at site 1 is likely a function of increased evapotranspiration and thus, drier antecedent soil moisture conditions at the onset of the NAM season, as indicated by decreased VWC in shallow soils from 6 instrumented pedons in the ZOB immediately before monsoon storms began compared to wetter soils during spring snowmelt and fall storms (Figure 4). This agrees with previous studies in the VCNP, which found that soil moisture was lowest in early summer after soil moisture from snowmelt had receded and it increased after the arrival of monsoon storms (Vivoni et al., 2008; Molotch et al., 2009). Furthermore, Zapata-Rios et al. (2015a) found that NDVI in the VCNP increased during the NAM season suggesting that precipitation was partitioned to plant use during monsoon rains and was not available to recharge groundwater stores. Moreover, smaller, sporadic precipitation during summer monsoon storms, increased evapotranspiration due to higher temperatures (Figure 3A), and increased plant use create a wetting and drying effect in shallow soils that can be seen as small fluctuations in VWC (Figure 4). This effect likely inhibits infiltration of water into the deep subsurface and agrees with Langston et al. (2015)'s model of unsaturated zone flow in two seasonally snow covered hillslopes in Colorado, which found that dry periods between low intensity precipitation and infiltration events inhibited recharge because of the need for shallow soil to re-wet after each precipitation event.

4.2 Water routing in unsaturated zone

Precipitation inputs differ before each neutron probe measurement (cumulative precipitation of 163.18 mm between June and August neutron probe measurements, 67.55 mm between August and October measurements, and 162.58 mm between October and February measurements; Figure 6 top); however, water content is nearly identical in the top 4 mbgs in three of the four profiles for site 2 wells and in all site 3 data collection events (Figure 6 bottom). We hypothesize that the response seen at site 2 in the October survey is a function of both the slightly larger precipitation depth prior to this survey and the wetter shallow soil conditions preceding the survey as compared to the conditions preceding the other three surveys. Higher frequency sampling during wet season are needed to determine the impact of precipitation depth and the potential for precipitation thresholds to induce vertical flow. Perhaps temporal changes in water content with depth were missed because of the sporadic timing of neutron probe surveys due to the arduous transportation and permitting issues involved with the use of this instrument. While it does not appear that water content profiles with depth captured progressive enrichments in rock moisture as seen by Salve et al. (2012) and Rempe and Dietrich (2018), they do indicate that the minimum dry season rock moisture storage is consistent across dry seasons, suggest differences in water routing, and identify lithologic discontinuities in the subsurface.

Neutron probe surveys show small shifts in water content with depth that are likely associated with small scale heterogeneities in bulk density created by the lithologic discontinuities in volcanic collapse breccia deposits, variable degrees of ash consolidation, welding, and secondary mineral precipitation, which are evident in quantitative mineralogical analyses (Moravec et al., 2018). For instance, well logs showed that a thin layer of coarse gravel-like material underlies the soil at site 2 wells, which is expected to drain quickly (high permeability) and retain little water (low porosity). At the depth corresponding to that gravel-like layer from 1.5 to 2.3 mbgs, water content across all times recedes quickly (Figure 6, borehole 2B) or remains constant (borehole 2C) before increasing rapidly just above the water table of the shallow aquifer. Salve et al. (2012) also found that moisture content variation from neutron probe surveys in weathered argillite were strongly linked to changes in material properties with depth, which suggested different flow processes through the unsaturated zone. Here, layers of increased water content (like that from 9 to 11 mbgs in well 2B) above layers of relatively lower water content (like that of 12 to 13.5 mbgs in well 2B) are indicative of subsurface lateral flow through more saturated, more conductive media that can be seen in Figure 6.

Evidence of vertical infiltration is also seen in the site 2 wells. The marked change in shape (increased water content from 1 to 4 mbgs) of the October water content profile suggests vertical infiltration and subsequent recharge to the shallow aquifer. Analysis of well 2D hydrograph (Figure 3F) confirms that this October neutron probe survey was completed while the shallowwater table was rising. Despite similar shallowwater table depths for all four surveys (2.7 mbgs on 6/27/17, 2.9 mbgs on 8/15/17, 2.9 mbgs on 10/12/17, and 3.2 mbgs on 2/6/18), the October survey was the only survey that corresponds with a rising rather than receding water table (Figure 3F) and is the only water content profile that captured vertical infiltration of recharge to the shallow aquifer. Furthermore, the wet October profile returns to dry conditions within the top 4 m in February and February water content beneath 4 m exceeds that of previous surveys, which suggests that water drains vertically at depths greater than 4 mbgs in February.

Geologic maps of the Valles Caldera (Goff et al., 2011) indicate that a concealed fault bisects the ZOB and it appears that site 3 wells were drilled immediately next to (possibly within) the fault zone, which coincides with the convergent outlet of the ZOB (Figure 1). This is likely why site 3 wells did not produce water in the time period of this study (Figure 2). Furthermore, water content is nearly identical across all four measurement events in borehole 3B (Figure 6). Despite being located in a convergent zone subjected to seasonal wetland saturated conditions at the land surface, neutron probe surveys do not indicate that water infiltrates vertically in site 3. Rather, data suggest that water moves laterally in the subsurface as indicated by the three zones of increased water content seen in Figure 6. This is further supported by high clay content (up to 50%) observed below 1.5 m depth at site 3 (Moravec et al. 2018), which likely impedes vertical infiltration and induces lateral flow in the subsurface.

4.3 Contribution of distinct groundwater stores to streamflow In the same headwater catchment in the JRB-CZO, Olshansky et al. (2018) observed temporal changes in major ion concentrations of soil, surface, and ground water during spring snowmelt 2017. They found pulses of high Si concentrations during the falling limb of surface water hydrographs that were hypothesized to result from increasing groundwater contributions during receding surface flows because surface water Si concentrations were similar to those of shallow groundwater (Well 2D). However, surface water concentrations of other major ions (Ca^{2+}, Na^{+}, Mg^{2+}, Mn, and SO_4^{2-}) did not coincidentally rise despite higher shallow groundwater concentrations of those ions compared to Si, which suggests, instead, a deeper source of groundwater to La Jara streams. Herein, we present further evidence that the deep groundwater source to La Jara and ZOB surface water is the deep welded tuff aquifer system found throughout the greater La Jara catchment and represented at site 1 wells.

High Ca^{2+}/Mg^{2+} molar ratios of shallow groundwater (Well 2D; Figure 8) are attributed to calcite dissolution, which is only present in the shallow subsurface at site 2 and leads to increased Ca^{2+} concentrations, but does not impact Mg^{2+} concentrations. The clear separation of Ca^{2+}/Mg^{2+} molar ratios in shallow (Well 2D) and deep groundwater (Wells 1A, 1B, 2A, 2B, and 2C) and the overlap of surface water Ca^{2+}/Mg^{2+} molar ratios with those of deeper groundwater (Figure 8A) suggests that the shallow aquifer does not contribute substantial volumes to surface flow, but instead deep groundwater is the dominant source of streamflow.

The dissolution of calcite in the shallow aquifer also leads to higher DIC concentrations in waters in the ZOB (Table 2; Appelo and Postma, 2005). Higher DIC concentrations in all site 2 waters is consistent with some degree of vertical connection between site 2 wells that, in turn, suggests the suspected confining layer beneath the shallow aquifer acts as more of an aquitard than aquiclude. The Ca^{2+}/Mg^{2+} molar ratios and DIC concentrations of surface waters are very similar to those of site 1 groundwaters (Figure 8B), which again indicates that deep groundwater from site 1 wells is more representative of groundwaters that contribute to La Jara stream. The welded tuff rock type (Figure 1) of site 1 wells is also more representative of the geology, by volume, throughout the greater La Jara catchment.

Temporal analysis of major ion chemistry indicates that deep groundwater from fractured tuff (Site 1) sustains stream baseflow as streamflow concentrations and trends in concentrations over time are consistent with site 1 groundwater concentrations. In contrast, pronounced changes in shallow site 2 groundwater (Wells 2D and 2C) major ion chemistry are not reflected in streamflow concentrations over time, which suggests that shallow groundwater represents only a small volumetric contribution to streamflow. Furthermore, recent work by Olshansky et al. (2018) found that soil water was an important contributor to surface water during spring snowmelt 2017 and may explain the subtle trends in Ca^{2+} and DIC concentrations of surface waters, particularly ZOB surface water which was correlated with soil P_{CO2} concentrations, at the onset of snowmelt.

4.4 Mix of old and young snowmelt dominated waters

Snowmelt is the dominant source of recharge to all groundwater stores in this study as the $\delta^{18}O$ and $\delta^{2}H$ values of surface water and groundwater plot much closer to the volume weighted mean (VWM) of snow (Gustafson, 2008) than to the VWM of summer precipitation (Zapata-Rios et al., 2015b) (Figure 9). Furthermore, the detection of tritium in groundwater from each sampled well indicates a component of modern recharge to each groundwater store, which agrees with previous work that found springs surrounding Redondo Peak are composed of modern water (Zapata-Rios et al., 2015b). The presence of tritium in groundwater suggests that snowmelt slowly infiltrates into all groundwater stores (Figure 10). However, radiocarbon analysis of wells 2D and 2C also indicates the presence of much older waters (corrected ages of 621 and 2050, respectively; Table 3) in these shallow groundwater reservoirs (Figure 10). The detection of tritium and less than 100 pmC in these wells suggests a mixture of old and young waters (Bethke and Johnson, 2008; Jasechko et al., 2017); that is expected to persist in each groundwater store.

Decreasing tritium content with depth from 2D to 2C to 2B (Table 3) agrees with previous studies that have suggested residence times increase with depth (Zapata-Rios et al., 2015b). This trend along with the distinct Ca^{2+}/Mg^{2+} molar ratios and DIC concentrations from the presence of shallow calcite deposits in site 2 wells is consistent with a vertical connection between the three shallowest site 2 wells. However, increased tritium content in well 2A (closer to that of site 1 than other site 2 wells) suggests that 2A is not vertically connected to the above site 2 wells and, instead, is likely laterally connected to younger waters upgradient.

The few samples that plot to the right of the meteoric water line may be related to evaporation and/or the presence of geothermal waters. The slope of the evaporation trend (m=3.4) is consistent with the slope of evaporation trends seen in arid environments like southern Arizona and northern Mexico (Gray, 2018; Zamora, 2018). The timing of the lower surface water $\delta^{18}O$ and $\delta^{2}H$ values is indicative of evaporative enrichment; however, the sporadic timing during surface water baseflow of the lower $\delta^{18}O$ and $\delta^{2}H$ values for all groundwaters is surprising (Supplemental Figure 2).

The second possible explanation of this enrichment trend is the presence of geothermal waters in the ZOB. The observed enrichment trend is consistent with that seen by Vautaz and Goff (1986) from geothermal waters sampled from lower elevations in the Valles Caldera and surrounding area. However, analysis of other geothermal water indicators (pCO_2 and temperature) does not suggest the presence of geothermal waters in the ZOB. Furthermore, SO_4^{2-} and Cl^- concentrations (data not shown) are several orders of magnitude lower than those of known geothermal waters from Vuataz and Goff (1986).

In summary, we propose a schematic model (Figure 10) to conceptualize the details of hydrologic structure and hydrologic function at two contrasting hillslopes within the ZOB (Sites 1 and 2). Site 2 has multiple, separate stores of groundwater across depth that are distinct from each other and distinct from deep groundwater stores at site 1. All groundwater is recharged via snowmelt and seasonal differences in hydrologic response to precipitation inputs exist at both sites with less pronounced response to summer monsoons at both sites linked to drier antecedent shallow soil moisture at the onset of NAM season. There is evidence of vertical infiltration and subsurface lateral flow at site 2 and a mix of young and older waters, which are expected to persist across all groundwater stores. The fracture density at site 1 is approximately 5 times greater than at site 2 and the CZ structure and architecture of site 1 is most representative of the greater La Jara catchment. Deep groundwater from the fractured aquifer system at site 1 is hydrologically connected to streamflow and site 1 deep groundwater chemistry is most representative of water contributing to streamflow while the distinct chemical signature of shallow groundwater from site 2 is not seen in streamflow. This study is not able to discern where the site 2 shallow groundwater drains, but it is possible that it transmits to streamflow in a quantity too low to detect because of dilution. The lateral extent of the shallow aquifer is not known and therefore, calculations of the volume of water in that aquifer cannot be made at this time.

5 Conclusions

There are multiple separate stores of groundwater in the subsurface of the ZOB at the JRB-CZO. Major ion chemistry show that these groundwater stores are chemically distinct, while δ^{18}O and δ^{2}H values indicate that snowmelt is the dominant source of recharge to all groundwater. Furthermore, seasonal differences in hydrologic response to periodic precipitation inputs, including a less pronounced response to summer monsoons, are seen in groundwaters within the ZOB. Tritium concentrations and radiocarbon analysis indicate that groundwaters are a mix of modern recharge with older waters. The path and timing of water moving through the subsurface is influenced by subsurface structure, which is exemplified by variable water contents with depth as a function of within-catchment lateral and vertical lithologic variation. The shallow aquifer at site 2 resides in a disconnected collapse breccia deposit of different geology from the other wells, is geochemically different from La Jara stream water, and does not respond to the pressure pulse associated with increasing streamflow and rising water table in the deep site 1 aquifer system, which suggests that shallow groundwater does not contribute significantly to streamflow.

We conclude that the fractured rock site 1 architecture is most representative of the CZ volume that dominantly contributes to La Jara streamflow across the water year. The similarity in shape and timing of well 1A and surface water hydrographs results from pressure pulse propagation through the transmissive, low storage fractured aquifer system. Furthermore, the clear similarities in major ion chemistry confirm the connection between La Jara stream and site 1 groundwater. Surprisingly, deep groundwater from site 1 wells appear to be more chemically-representative of waters that contribute to La Jara stream and more representative of the structure (geology, fractured aquifer system, and greater depth to water table) and function (hydrologic response, solute fluxes, and water routing) of the CZ in the greater La Jara catchment, suggesting that deep groundwater from the fractured aquifer system, rather than shallow groundwater, sustains stream baseflow. Further, we suggest that the deep subsurface flow paths observed in the JRB-

CZO are likely a signature of snow dominated volcanic catchments transferable to other deeply fractured extrusive bedrock systems, which highlights the need to consider deeper groundwater processes in integrated hydrologic models.

The dominant contribution of deep groundwater to surface flows and the hydraulic connection between the fractured bedrock aquifer system and streamflow may suggest that deep groundwater stores in fractured bedrock aquifers are sensitive to changes in climatic drivers of streamflow like shifts in precipitation magnitude and timing, as predicted in the southwestern United States. We assert that this study emphasizes the utility of interdisciplinary research to discern the distribution of groundwater stores, their connection to streamflow, and the underlying impact of CZ architecture on hydrologic response to climatic drivers. Furthermore, it highlights the need to better characterize the deep subsurface of mountain systems by transferring this approach to other complex settings that challenge and advance the current understanding of subsurface hydrologic systems around the world. This study provides a template of how to bring together multiple lines of evidence to simultaneously examine both, CZ architecture and hydrology, through hydrometric, geophysical, geochemical, and residence time analyses.

Acknowledgements

This research was funded by the U.S. National Science Foundation grants EAR-0724958 and EAR-1331408, which support the Catalina-Jemez River Basin Critical Zone Observatories. Additional funding was provided by a Geological Society of America Student Research Grant awarded to A. White. We also thank the Continental Scientific Drilling Coordination Office and the National Lacustrine Core Facility (LacCore) for their help with collecting, subsampling, and analyzing intact cores. We are grateful to Mary Kay Amistadi, Tim Corley, Nicole Vicenti, Adam Weber, Mark Losleben, and Adam Killebrew for their assistance with chemical analyses and field work.

Author Contribution

AW performed the data analysis, developed the conceptual framework, and wrote the manuscript with assistance from JM, TF, TM, JC, YO, and BM. AW collected and processed samples with help from BM, AS, and BP. JM and JC supervised the project.

References

Anderson, S. P., von Blanckenburg, F., and White, A. F.: Physical and chemical controls on the critical zone, Elements, 3, 315-319, https://doi.org/10.2113/gselements.3.5.315, 2007.

Anderson, S. P., Bales, R. C., and Duffy, C. J.: Critical Zone Observatories: Building a network to advance interdisciplinary study of Earth surface processes, Mineralogical Magazine, 72, 7-10, https://doi.org/10.1180/minmag.2008.072.1.7, 2008.

Appelo, C. A. J., and Postma, D.: Geochemistry, Groundwater and Pollution, 2nd Ed., CRC press, New York, 2005.

Bailey, R. A., Smith, R. L., and Ross, C. S.: Stratigraphic Nomenclature of Volcanic Rocks in the Jemez Mountains, New Mexico, Geological Survey Bulletin 1274-P: Contributions to Stratigraphy, US Geological Survey, 1969.

Barnett, T. P., Adam, J. C., and Lettenmaier, D. P.: Potential impacts of a warming climate on water availability in snow-dominated regions, Nature, 438, 303-309, doi:10.1038/nature04141, 2005.

Bethke, C. M., and Johnson, T. M.: Groundwater age and groundwater age dating, Annu. Rev. Earth Planet. Sci., 36, 121-152, https://doi.org/10.1146/annurev.earth.36.031207.124210, 2008.

Beven, K. J., and Kirkby, M. J.: A physically based, variable contributing area model of basin hydrology, Hydrological Sciences Journal, 24, 43-69, https://doi.org/10.1080/02626667909491834, 1979.

Bevington, P. R., and Robinson, D. K.: Data Reduction and Error Analysis for the Physical Sciences, McGraw-Hill, New York, 1992.

Bhanja, S. N., Zhang, X., and Wang, J.: Estimating long-term groundwater storage and its controlling factors in Alberta, Canada, Hydrology and Earth System Sciences, 22, 6241-6255, https://doi.org/10.5194/hess-22-6241-2018, 2018.

Brantley, S. L., White, T. S., White A. F., Sparks, D., Richter, D., Pregitzer, K., Derry L., Chorover, J., Chadwick, O., April, R., Anderson, S., and Amundson, R.: Frontiers in exploration of the critical zone, an NSF-sponsored workshop, National Science Foundation, 2006.

Brantley, S. L., Goldhaber, M. B., and Ragnarsdottir, K. V.: Crossing disciplines and scales to understand the critical zone, Elements, 3, 307-314, https://doi-org.ezproxy4.library.arizona.edu/10.2113/gselements.3.5.307, 2007.

Brantley, S. L., Lebedeva, M. I., Balashov, V. N., Singha, K., Sullivan, P. L., and Stinchcomb, G.: Toward a conceptual model relating chemical reaction fronts to water flow paths in hills, Geomorphology, 277, 100-117, https://doi.org/10.1016/j.geomorph.2016.09.027, 2017.

Brooks, P. D., Chorover, J., Fan, Y., Godsey, S. E., Maxwell, R. M., McNamara, J. P., and Tague, C.: Hydrological partitioning in the critical zone: Recent advances and opportunities for developing transferable understanding of water cycle dynamics, Water Resources Research, 51, 6973-6987, https://doi.org/10.1002/2015WR017039, 2015.

Broxton, P. D., Troch, P. A., and Lyon, S. W.: On the role of aspect to quantify water transit times in small mountainous catchments, Water Resources Research, 45, https://doi.org/10.1029/2008WR007438, 2009.

Butler Jr, J. J., and Healey, J. M.: Relationship between pumping-test and slug-test parameters: Scale effect or artifact?, Groundwater, 36, 305-312, 1998.

Butler, J. J.: The design, performance, and analysis of slug tests, 2nd Ed., CRC Press, New York, 2015.

Chorover, J., Kretzschmar, R., Garcia-Pichel, F., and Sparks, D. L.: Soil biogeochemical processes within the critical zone, Elements, 3, 321-326, https://doi.org/10.2113/gselements.3.5.321, 2007.

Chorover, J., Troch, P. A., Rasmussen, C., Brooks, P. D., Pelletier, J. D., Breshars, D. D., Huxman, T. E., Kurc, S. A., Lohse, K.A., McIntosh, J. C., Meixner, T. Shaap, M. G., Litvak, M. E., Perdrial, J., Harpold, A. and Durcik, M.: How water, carbon, and energy drive critical zone evolution: The Jemez-Santa Catalina Critical Zone Observatory, Vadose Zone Journal, 10, 884-899, https://doi.org/10.2136/vzj2010.0132, 2011.

Clark, I., and Fritz, P.: Environmental Isotopes in Hydrogeology. CRC Press, New York, 1997.

Dershowitz, W. S., and Herda, H. H.: Interpretation of fracture spacing and intensity. In The 33th US Symposium on Rock Mechanics (USRMS). American Rock Mechanics Association, 1992.

Dralle, D. N., Hahm, W. J., Rempe, D. M., Karst, N. J., Thompson, S. E., and Dietrich, W. E.: Quantification of the seasonal hillslope water storage that does not drive streamflow, Hydrological processes, 32, 1978-1992, https://doi.org/10.1002/hyp.11627, 2018.

Drever, J.I.: The Geochemistry of Natural Waters: Surface and Groundwater Environments, 3rd Ed., Prentice Hall, New Jersey, 1997.

Duffield, G. M.: AQTESOLV for Windows Version 4.5 User's Guide. HydroSOLVE, Reston, VA, 2007.

Eastoe, C. J., Watts, C. J., Ploughe, M., and Wright, W. E.: Future use of tritium in mapping Pre-Bomb groundwater volumes, Groundwater, 50, 87-93, https://doi.org/10.1111/j.1745-6584.2011.00806.x, 2012.

Farvolden, R. N.: Geologic controls on ground-water storage and base flow, Journal of Hydrology, 1, 219-249, 1963.

Flinchum, B. A., Holbrook, S. W., Rempe, D., Moon, S., Riebe, C. S., Carr, B. J., Hayes, J.L., St. Clair, J., and Peters, M. P.: Critical zone structure under a granite ridge inferred from drilling and three-dimensional seismic refraction data, Journal of Geophysical Research: Earth Surface, 123, 1317-1343, https://doi.org/10.1029/2017JF004280, 2018.

Freeze, R. A.: Role of subsurface flow in generating surface runoff: 1. Base flow contributions to channel flow, Water Resources Research, 8, 609-623, 1972.

Frisbee, M. D., Phillips, F. M., White, A. F., Campbell, A. R., and Liu, F.: Effect of source integration on the geochemical fluxes from springs, Applied Geochemistry, 28, 32-54, https://doi.org/10.1016/j.apgeochem.2012.08.028, 2013.

Gardner, C. M., Robinson, D. A., Blyth, K., and Cooper, J. D.: Soil water content, in: Soil and environmental analysis: Physical methods, 2nd Ed., edited by: Smith, K. A., and Mullins, C. E., . Marcel Dekker, Inc., New York, 1-64, 2000.

Goff, F., Gardner, J. N., Reneau, S. L., Kelley, S. A., Kempter, K. A., and Lawrence, J. R.: Geologic map of the Valles Caldera, Jemez Mountains, New Mexico, Geologic Map 79, New Mexico Bureau of Geology and Mineral Resources, 2011.

Gray, E. L.: Using water isotopes and solute chemistry to investigate the hydrology of surface water in the Cienega Creek Watershed, MS Thesis, The University of Arizona, 2018.

Gustafson, J. R.: Quantifying spatial variability of snow water equivalent, snow chemistry, and snow water isotopes: Application to snowpack water balance, MS Thesis, The University of Arizona, 2008.

Healy, D., Rizzo, R. E., Cornwell, D. G., Farrell, N. J., Watkins, H., Timms, N. E., Gomez-Rivas, E., and Smith, M.: FracPaQ: A MATLAB™ toolbox for the quantification of fracture patterns, Journal of Structural Geology, 95, 1-1, https://doi.org/10.1016/j.jsg.2016.12.003, 2017.

Holbrook, W. S., Riebe, C. S., Elwaseif, M., L. Hayes, J. L., Basler-Reeder, K., Harry, D. L., Malazian, A., Dosseto, A., Hartsough, P. C., and W. Hopmans, J. W.: Geophysical constraints on deep weathering and water storage potential in the Southern Sierra Critical Zone Observatory, Earth Surface Processes and Landforms, 39, 366-380, https://doi.org/10.1002/esp.3502, 2014.

Hulen, J. B. and Nielson, D. L.: Evolution of the Western Valles Caldera Complex, New Mexico – Evidence from intracaldera sandstones, breccias, and surge deposits, Journal of Geophysical Research-Solid Earth and Planets, 96, 8127-8142, https://doi.org/10.1029/91JB00374, 1991.

Hutchinson, D. G., and Moore, R. D.: Throughflow variability on a forested hillslope underlain by compacted glacial till, Hydrological processes, 14, 1751-1766, 2000.

Hyder, Z., Butler, J. J., McElwee, C. D., and Liu, W.: Slug tests in partially penetrating wells, Water Resources Research, 30, 2945-2957, https://doi.org/10.1029/94WR01670, 1994.

Jasechko, S., Perrone, D., Befus, K. M., Cardenas, M. B., Ferguson, G., Gleeson, T., Luijendijk, E., McDonnell, J. J., Taylor, R. G., Wada, Y., and Kirchner, J. W.: Global aquifers dominated by fossil groundwaters but wells vulnerable to modern contamination, Nature Geoscience, 10, 425-429, https://doi.org/10.1038/ngeo2943, 2017.

Kearl, P. M., Zinkl, R. J., Dexter, J. J., and Cronk, T.: Air permeability measurements of the unsaturated Bandelier Tuff near Los Alamos, New Mexico, Journal of Hydrology, 117, 225-240, https://doi.org/10.1016/0022-1694(90)90094-E, 1990.

Kelson, K. I., and Wells, S. G.: Geologic influences on fluvial hydrology and bedload transport in small mountainous watersheds, northern New Mexico, USA, Earth Surface Processes and Landforms, 14, 671-690, 1989.

Kim, H., Bishop, J. K. B., Dietrich, W. E., and Fung, I. Y.: Process dominance shift in solute chemistry as revealed by long-term high-frequency water chemistry observations of groundwater flowing through weathered argillite underlying a steep forested hillslope, Geochimica Et Cosmochimica Acta, 140, 1-19, https:doi.org/10.1016/j.gca.2014.05.011, 2014.

Kim, H., Dietrich, W. E., Thurnhoffer, B. M., Bishop, J. K. B., and Fung, I. Y.: Controls on solute concentration-discharge relationships revealed by simultaneous hydrochemistry observations of hillslope runoff and stream flow: The importance of critical zone structure, Water Resources Research, 53, 1424-1443, https://doi.org/10.1002/2016WR019722, 2017.

Kirchner, J. W., Feng, X., and Neal, C.: Catchment-scale advection and dispersion as a mechanism for fractal scaling in stream tracer concentrations, Journal of Hydrology, 254, 82-101, https://doi.org/10.1016/S0022-1694(01)00487-5, 2001.

Küsel, K., Totsche, K. U., Trumbore, S. E., Lehmann, R., Steinhäuser, C., and Herrmann, M.: How deep can surface signals be traced in the critical zone? Merging biodiversity with biogeochemistry research in a central German Muschelkalk landscape, Frontiers in Earth Science, 4, https://doi.org/10.3389/feart.2016.00032, 2016.

Langston, A. L., Tucker, G. E., Anderson, R. S., and Anderson, S. P.: Evidence for climatic and hillslope-aspect controls on vadose zone hydrology and implications for saprolite weathering, Earth Surface Processes and Landforms, 40, 1254-1269, https://doi.org/10.1002/esp.3718, 2015.

Liu, F., Parmenter, R., Brooks, P., Conklin, M., and Bales, R.: Seasonal and interannual variation of streamflow pathways and biogeochemical implications in semi-arid, forested catchments in Valles Caldera, New Mexico, Ecohydrology, 1, 239-252, https://doi.org/10.1002/eco.22, 2008a.

Liu, F., Bales, R. C., Conklin, M. H., and Conrad, M. E.: Streamflow generation from snowmelt in semi-arid, seasonally snow-covered, forested catchments, Valles Caldera, New Mexico, Water Resources Research, 44, https://doi.org/10.1029/2007WR006728, 2008b.

Longmire, P., Dale, M., Counce, D., Manning, A., Larson, T., Granzow, K., Gray, R., and Newman, B.: Radiogenic and stable isotope and hydrogeochemical investigation of groundwater, Pajarito Plateau and surrounding areas, New Mexico (No. LA-14333). Los Alamos National Laboratory (LANL), Los Alamos, NM, 153 pp., 2007.

Manga, M.: Using springs to study groundwater flow and active geologic processes, Annual Review of Earth and Planetary Sciences, 29, 201-228, https://doi.org/10.1146/annurev.earth.29.1.201, 2001.

Manning, A. H.: Ground-water temperature, noble gas, and carbon isotope data from the Española Basin, New Mexico, Scientific Investigations Report 2008-5200, U. S. Geological Survey, Santa Fe, NM, 78 pp., 2009.

Manning, A. H., and J. S. Caine.: Groundwater noble gas, age, and temperature signatures in an Alpine watershed: Valuable tools in conceptual model development, Water Resources Research, 43, https://doi.org/10.1029/2006WR005349, 2007.

Markovich, K. H., Manning, A. H., Condon, L. E., and McIntosh, J. C.: Mountain-block recharge: A review of current understanding, Water Resources Research, Accepted.

Mauldon, M., Dunne, W. M., and Rohrbaugh Jr, M. B.: Circular scanlines and circular windows: new tools for characterizing the geometry of fracture traces, Journal of Structural Geology, 23, 247-258, https://doi.org/10.1016/S0191-8141(00)00094-8, 2001.

McDonnell, J. J.: Beyond the water balance, Nature Geoscience, 10, 396, https://doi.org/10.1038/ngeo2964, 2017.

McGuffy, C.: The role of initial porosity in regolith formation in igneous rocks, MS Thesis, University of Wyoming, 2017.

McGuire, K. J., McDonnell, J. J., Weiler, M., Kendall, C., McGlynn, B. L., Welker, J. M., and Seibert, J.: The role of topography on catchment-scale water residence time, Water Resources Research, 41, https://doi.org/10.1029/2004WR003657, 2005.

McIntosh, J. C., Schaumberg, C., Perdrial, J., Harpold, A., Vázquez-Ortega, A., Rasmussen, C., Vinson, D., Zapata-Rios, X., Brooks, P. D., Meixner, T., Pelletier, J., Derry, L., & Chorover, J.: Geochemical evolution of the critical zone across variable time scales informs concentration-discharge relationships: Jemez river basin critical zone observatory, Water Resources Research, 53, 4169-4196, https://doi.org/10.1002/2016WR019712, 2017.

Molotch NP, Brooks PD, Burns SP, Litvak M, Monson RK, McConnell JR, and Musselman K.: Ecohydrological controls on snowmelt partitioning in mixed-conifer sub-alpine forests, Ecohydrology, 2, 129–142, https://doi.org/10.1002/eco.48, 2009.

Mook , W. G., Bommerson, J. C. and Staverman, W. H.: Carbon isotope fractionation between dissolved bicarbonate and gaseous carbon dioxide, Earth and Planetary Science Letters, 22, 169-176, 1974.

Moravec, B., White, A., Root, R., McIntosh, J., and Chorover, J.: Deconvolving legacy and contemporaneous weathering in a porphyritic rhyolite and rhyolitic tuff dominated upland catchment, Valles Caldera, New Mexico, in: Proceedings of the GSA Annual Meeting, Indianapolis, Indiana, USA, 4-7 November 2018, 240-5, 2018.

Mwakalila, S., Feyen, J., and Wyseure, G.: The influence of physical catchment properties on baseflow in semi-arid environments, Journal of Arid Environments, 52, 245-258, https://doi.org/10.1006/jare.2001.0947, 2002.

Olshansky, Y., White, A., Moravec, B., McIntosh, J., and Chorover, J.: Subsurface pore water contributions to stream concentration-discharge relations across a snowmelt hydrograph, Frontiers in Earth Science, 6, https://doi.org/10.3389/feart.2018.00181, 2018.

Pearson, F. J.: Use of C-13/C-12 ratios to correct radiocarbon ages of material initially diluted by limestone, Proceedings of the 6[th] International Conference on Radiocarbon and Tritium Dating, Pullman, Washington, 357, 1965.

Pearson, F. J. and Hanshaw, B. B.: Sources of dissolved carbonate species in groundwater and their effects on carbon-14 dating, Isotope Hydrology 1970, IAEA Symposium 129, March 1970, Vienna: 271-286, 1970.

Perdrial, J. N., McIntosh, J., Harpold, A., Brooks, P. D., Zapata-Rios, X., Ray, J., Meixner, T., Kanduc, T., Litvak, M., Troch, P. A., and Chorover, J.: Stream water carbon controls in seasonally snow-covered mountain catchments: Impact of inter-annual variability of water fluxes, catchment aspect and seasonal processes, Biogeochemistry, 118, 273-290, https://doi.org/10.1007/s10533-013-9929-y, 2014.

Rempe, D. M.: Controls on critical zone thickness and hydrologic dynamics at the hillslope scale, Ph.D. dissertation, University of California, Berkeley, 2016.

Rempe, D. M., and Dietrich, W. E.: Direct observations of rock moisture, a hidden component of the hydrologic cycle, Proceedings of the National Academy of Sciences, 115, 2664-2669, https://doi.org/10.1073/pnas.1800141115, 2018.

Riebe, C. S., Hahm, W. J., and Brantley, S. L.: Controls on deep critical zone architecture: A historical review and four testable hypotheses, Earth Surface Processes and Landforms, 42, 128-156, https://doi.org/10.1002/esp.4052, 2017.

Rogers, D. B., and Gallaher, B. M.: The unsaturated hydraulic characteristics of the Bandelier Tuff (No. LA-12968-MS). Los Alamos National Lab, NM (United States), 1995.

Salve, R., Rempe, D. M., and Dietrich, W. E.: Rain, rock moisture dynamics, and the rapid response of perched groundwater in weathered, fractured argillite underlying a steep hillslope, Water Resources Research, 48, https://doi.org/10.1029/2012WR012583, 2012.

Scanlon, B. R.: Uncertainties in estimating water fluxes and residence times using environmental traces in an arid unsaturated zone, Water Resources Research, 2, 395–409, 2000.

Self, S., Goff, F., Gardner, J. N., Wright, J. V., and Kite, W. M.: Explosive Rhyolitic volcanism in the Jemez Mountains – Vent locations, caldera development, and relation to regional structure, Journal of Geophysical Research-Solid Earth and Planets, 91, 1779-1798, https://doi.org/10.1029/JB091iB02p017799, 1986.

Smyth, R. C., and Sharp Jr, J. M.: The hydrology of tuffs, Special Paper of the Geological Society of America, 408, 91-111, https://doi.org/10.1130/2006.2408(4.1), 2006.

Sophocleous, M., Townsend, M. A., Vogler, L. D., McClain, T. J., Marks, E. T., and Coble, G. R.: Experimental studies in stream-aquifer interaction along the Arkansas river in central Kansas — field testing and analysis, Journal of Hydrology, 98, 249-273, https://doi.org/10.1016/0022-1694(88)90017-0, 1988.

Sophocleous, M. A.: Stream-floodwave propagation through the great bend alluvial aquifer, Kansas: Field measurements and numerical simulations, Journal of Hydrology, 124, 207-228, https://doi.org/10.1016/0022-1694(91)90015-A, 1991a.

Sophocleous, M. A.: Combining the soilwater balance and water-level fluctuation methods to estimate natural groundwater recharge: Practical aspects, Journal of Hydrology, 124, 229-241, https://doi.org/10.1016/0022-1694(91)90016-B, 1991b.

Suckow, A.: The age of groundwater - definitions, models and why we do not need this term, Applied Geochemistry, 50, 222-230, https://doi.org/10.1016/j.apgeochem.2014.04.016, 2014.

Tóth, J.: A conceptual model of the groundwater regime and the hydrogeologic environment, Journal of Hydrology, 10, 164-176, 1970.

Vázquez-Ortega, A., Perdrial, J., Harpold, A., Zapata-Ríos, X., Rasmussen, C., McIntosh, J., Shapp, M., Pelletier, J. D., Brooks, P. D., Amistadi, M. K., and Chorover, J.: Rare earth elements as reactive tracers of biogeochemical weathering in forested rhyolitic terrain, Chemical Geology, 391, 19-32, https://doi.org/10.1016/j.chemgeo.2014.10.016, 2015.

Vázquez-Ortega, A., Huckle, D., Perdrial, J., Amistadi, M. K., Durcik, M., Rasmussen, C., McIntosh, J., and Chorover, J.: Solid-phase redistribution of rare earth elements in hillslope pedons subjected to different hydrologic fluxes, Chemical Geology, 426, 1-18, https://doi.org/10.1016/j.chemgeo.2016.01.001, 2016.

Viviroli, D., Dürr, H. H., Messerli, B., Meybeck, M., and Weingartner, R.: Mountains of the world, water towers for humanity: Typology, mapping, and global significance, Water Resources Research, 43, https://doi.org/10.1029/2006WR005653, 2007.

Vivoni E. R., Rinehart A. J., Mendez-Barroso L. A., Aragon C. A., Bisht G., Cardenas M. B., Engle E., Forman B. A., Frisbee M. D., Gutierrez-Jurado H. A., Hong S., Mahmood T. H., Tai K., and Wyckoff R. L.: Vegetation controls on soil moisture distribution in the Valles Caldera, New Mexico, during the North American monsoon, Ecohydrology, 1, 225–238, https://doi.org/10.1002/eco.11, 2008.

Vogel, J. C.: Carbon-14 dating of groundwater. In: Isotope Hydrology 1970, IAEA Symposium 129, March 1970, Vienna: 225-239, 1970.

Vuataz, F. D., and Goff, F.: Isotope geochemistry of thermal and nonthermal waters in the Valles Caldera, Jemez Mountains, northern New Mexico, Journal of Geophysical Research: Solid Earth, 91, 1835-1853, 1986.

Welch, C., Cook, P. G., Harrington, G. A., and Robinson, N. I.: Propagation of solutes and pressure into aquifers following river stage rise, Water Resources Research, 49, 5246-5259, https://doi.org/10.1002/wrcr.20408, 2013.

Welch, L.A., and D. M. Allen .: Hydraulic conductivity characteristics in mountains and implications for conceptualizing bedrock groundwater flow, Hydrogeology Journal, 22, https://doi.org/10.1007/s10040-014-1121-5, 2014.

Winter, T. C.: Ground water and surface water: A single resource. (No. 1139). Denver, CO, U.S. Dept. of the Interior, U.S. Geological Survey, 1998.

Winter, T. C.: Relation of streams, lakes, and wetlands to groundwater flow systems, Hydrogeology Journal, 7, 28-45, 1999.

Wolff, J. A., Brunstad, K. A., and Gardner, J. N.: Reconstruction of the most recent volcanic eruptions from the Valles Caldera, New Mexico, Journal of Volcanology and Geothermal Research, 199, 53-68, https://doi.org/10.1016/j.jvolgeores.2010.10.008, 2011.

Woods, R. A., Sivapalan, M., and Robinson, J. S.: Modeling the spatial variability of subsurface runoff using a topographic index, Water Resources Research, 33, 1061-1073, 1997.

Worthington, S. R. H.: Diagnostic tests for conceptualizing transport in bedrock aquifers, Journal of Hydrology, 529, 365-372, https://doi.org/10.1016/j.jhydrol.2015.08.002, 2015.

Zamora, H.: Environmental Isotope Geochemistry in Groundwaters of Southwestern Arizona, USA, and Northwestern Sonora, Mexico: Implications for Groundwater Recharge, Flow, and Residence Time in Transboundary Aquifers, Ph.D. dissertation, The University of Arizona, 2018.

Zapata-Rios, X., Brooks, P. D., Troch, P. A., McIntosh, J., and Guo, Q.: Influence of terrain aspect on water partitioning, vegetation structure and vegetation greening in high-elevation catchments in northern New Mexico: Terrain aspect, water partitioning, vegetation greening in high-elevation catchments, Ecohydrology, 9, 782-795, https://doi.org/10.1002/eco.1674, 2015a.

Zapata-Rios, X., McIntosh, J., Rademacher, L., Troch, P. A., Brooks, P. D., Rasmussen, C., and Chorover, J.: Climatic and landscape controls on water transit times and silicate mineral weathering in the critical zone, Water Resources Research, 51, 6036-6051, https://doi.org/10.1002/2015WR017018, 2015b.

Zuber, A., and Maloszewski, P.: Lumped parameter models, In: Mook, W. G. (Ed.), Environmental Isotopes in the Hydrological Cycle Principles and Applications, IAEA and UNESCO, Vienna, pp. 5-35, 2000.

Figures:

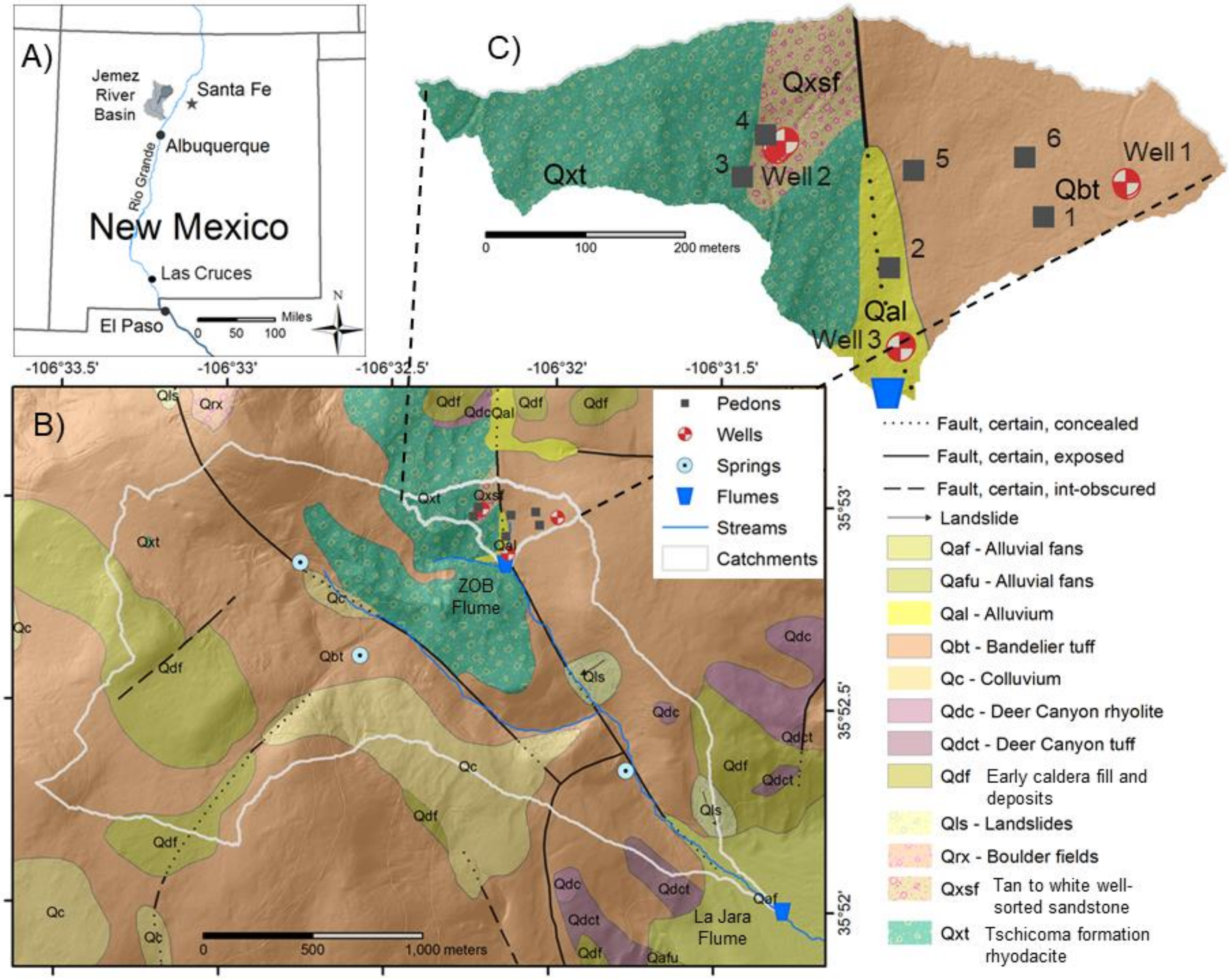

Figure 1: A) The Jemez River Basin Critical Zone Observatory (JRB-CZO) is located on the Valles Caldera National Preserve (VCNP) in northern New Mexico north of Albuquerque. B) Notice the geologic complexity of La Jara catchment and the Zero Order Basin (ZOB) and the location of surface water flumes and springs. C) Note the different geology of the three well sites, the location of the soil pedons in relation to the wells, and the fault at the site 3 well.

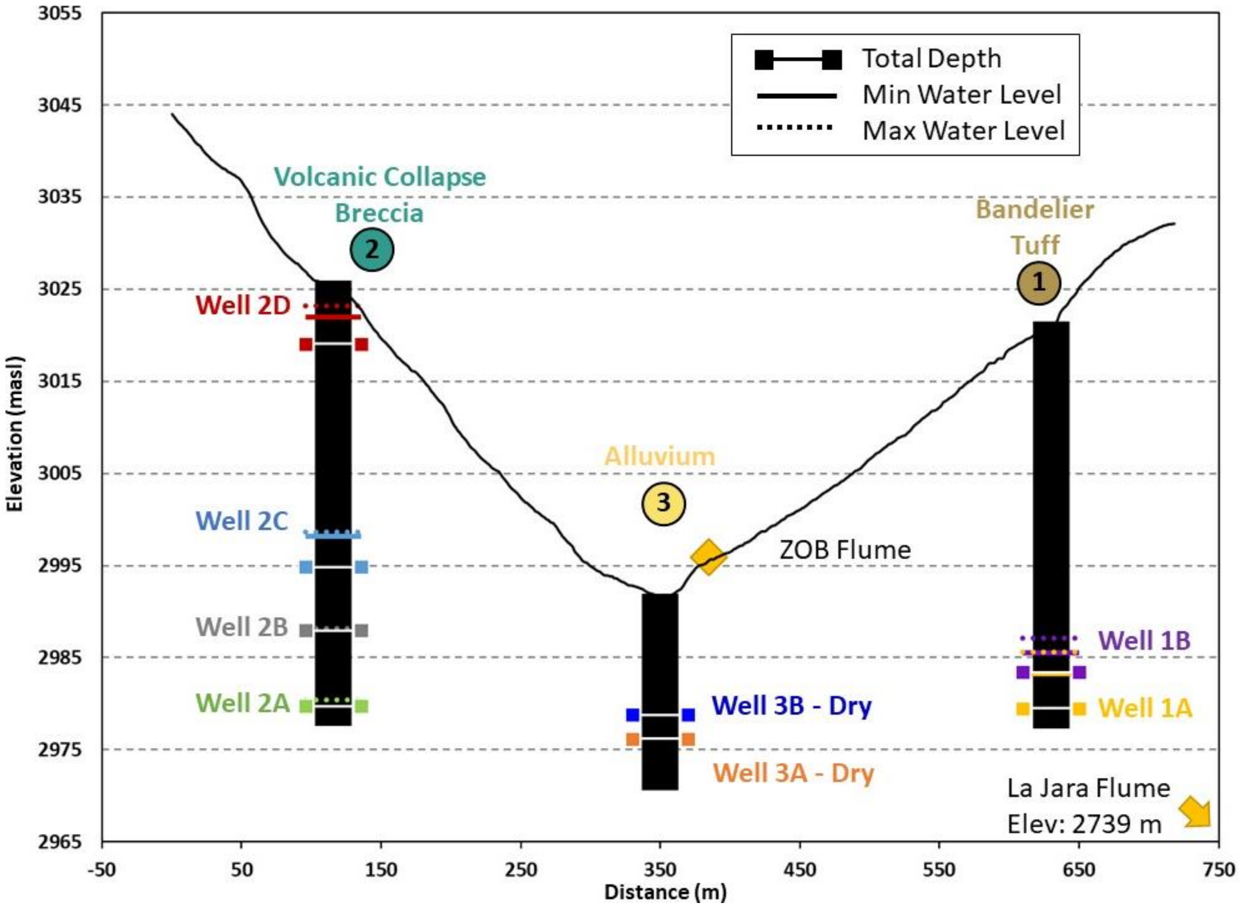

Figure 2: Profile of the nested groundwater wells within the ZOB showing surface topography, depth of wells, and seasonal changes in water column heights between maximum (dotted) and minimum (solid) in meters above sea level. Lines capped with square ends represent the base of each well. It is important to note the different rock type at each site, the suspected presence of a perched aquifer at well 2D, the disconnection between site 1 and 2 wells across the same elevation, as well as the absence of water in site 3 wells.

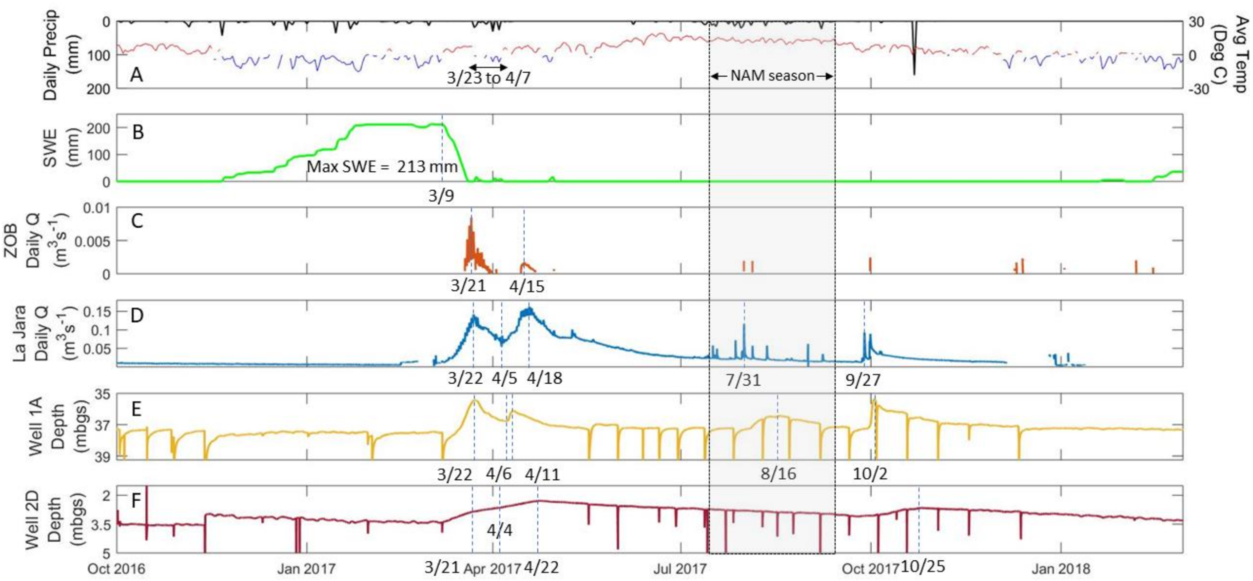

Figure 3: A) Daily averaged precipitation falls down from top axis. Average daily temperature is shown in red when temperatures are above zero and blue at or below zero degrees Celsius. B) Snow water equivalent (SWE) for WY 2017 reaches a maximum of 213 mm. C) Fifteen-min discharge of ZOB flume for WY 2017. D) Fifteen-min discharge of La Jara flume for WY 2017. E) Well 1A depth of water below ground surface from vibrating wire piezometer placed at 41.5 m below ground surface in fifteen-min intervals. Drops in water depth correspond to sample collection. F) Well 2D depth of water below ground surface from vibrating wire piezometer placed at 6.4 m below ground surface in fifteen-min intervals. Drops in water depth correspond to sample collection. The shaded region marks the timing of North American monsoon (NAM) season from July 15th through September 15th.

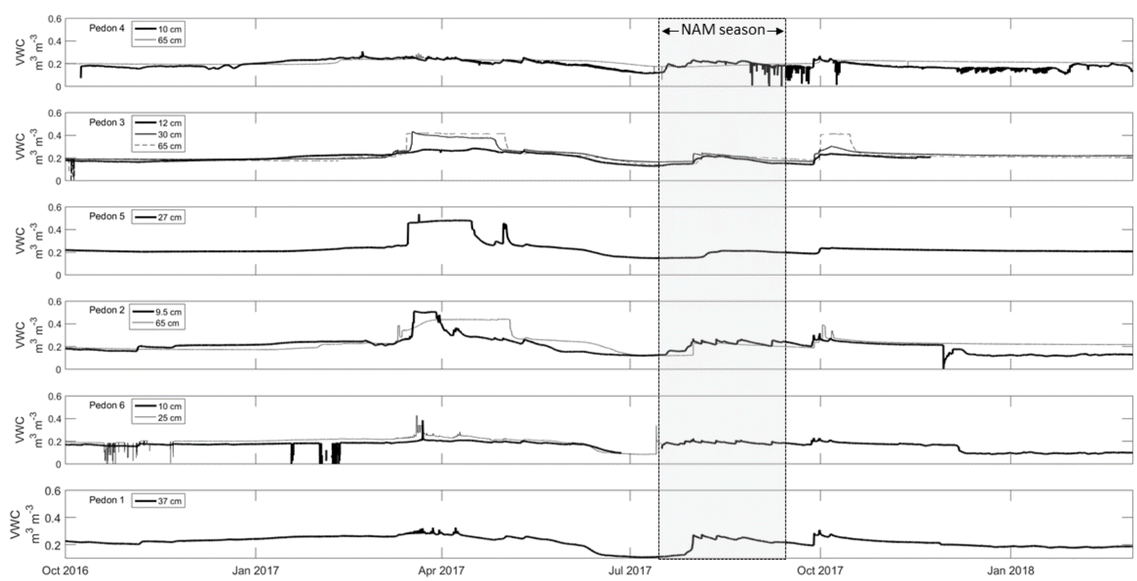

Figure 4. Volumetric water content (VWC) of six soil pedons in the ZOB. Pedons are grouped spatially with pedons 4 and 3 on the western side of the ZOB (near site 2 wells), pedons 5 and 2 in the convergent zone (near site 3 wells), and pedons 6 and 1 on the eastern side of the ZOB (near site 1 wells). The shaded region marks the timing of North American monsoon (NAM) season from July 15th through September 15th.

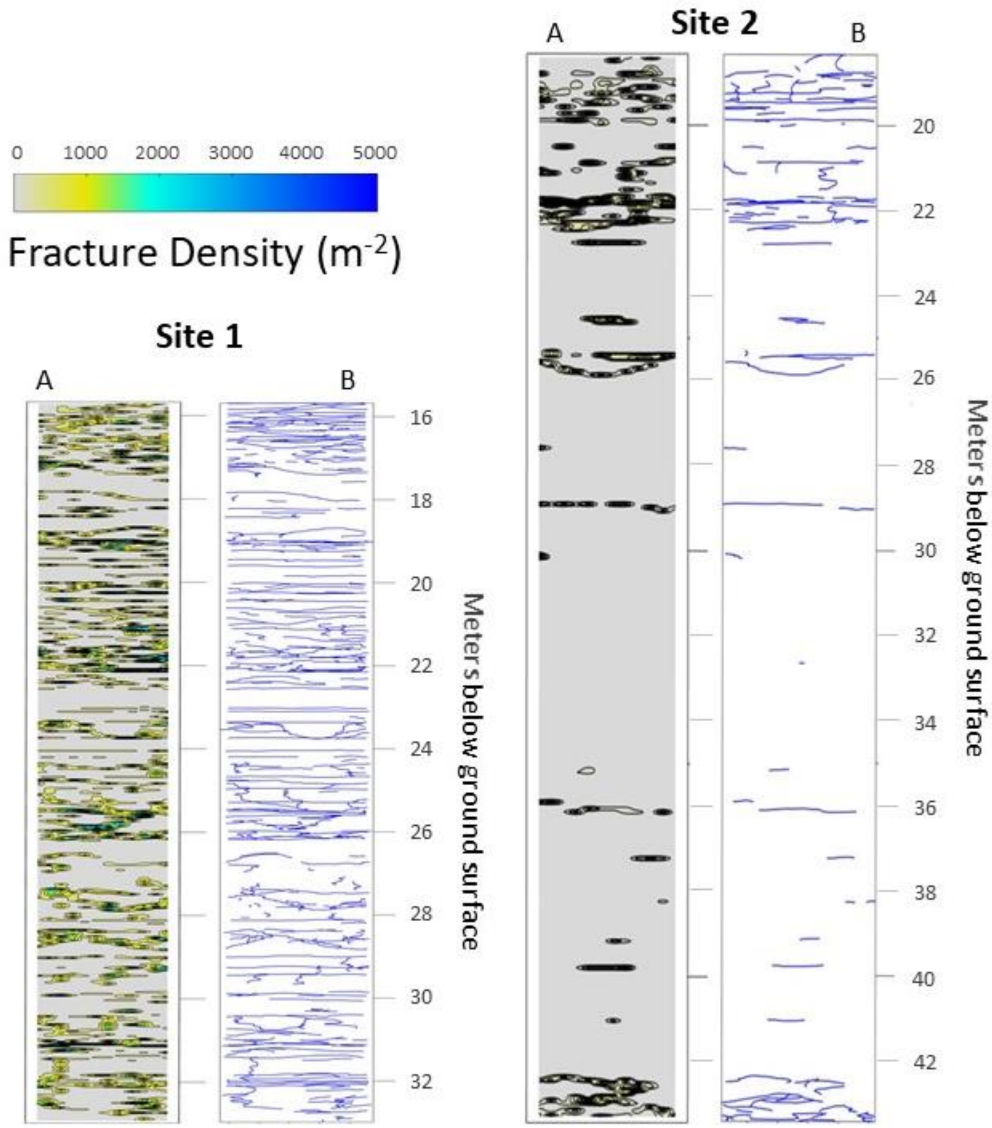

Figure 5: A) Fracture density of sites 1 (left) and 2 (right) in m^{-2}. Notice that fracture density is approximately 5 times greater in site 1 than 2 according to the color scale. B) Fracture traces of sites 1 (left) and 2 (right) show where fractures exist in meters below ground surface.

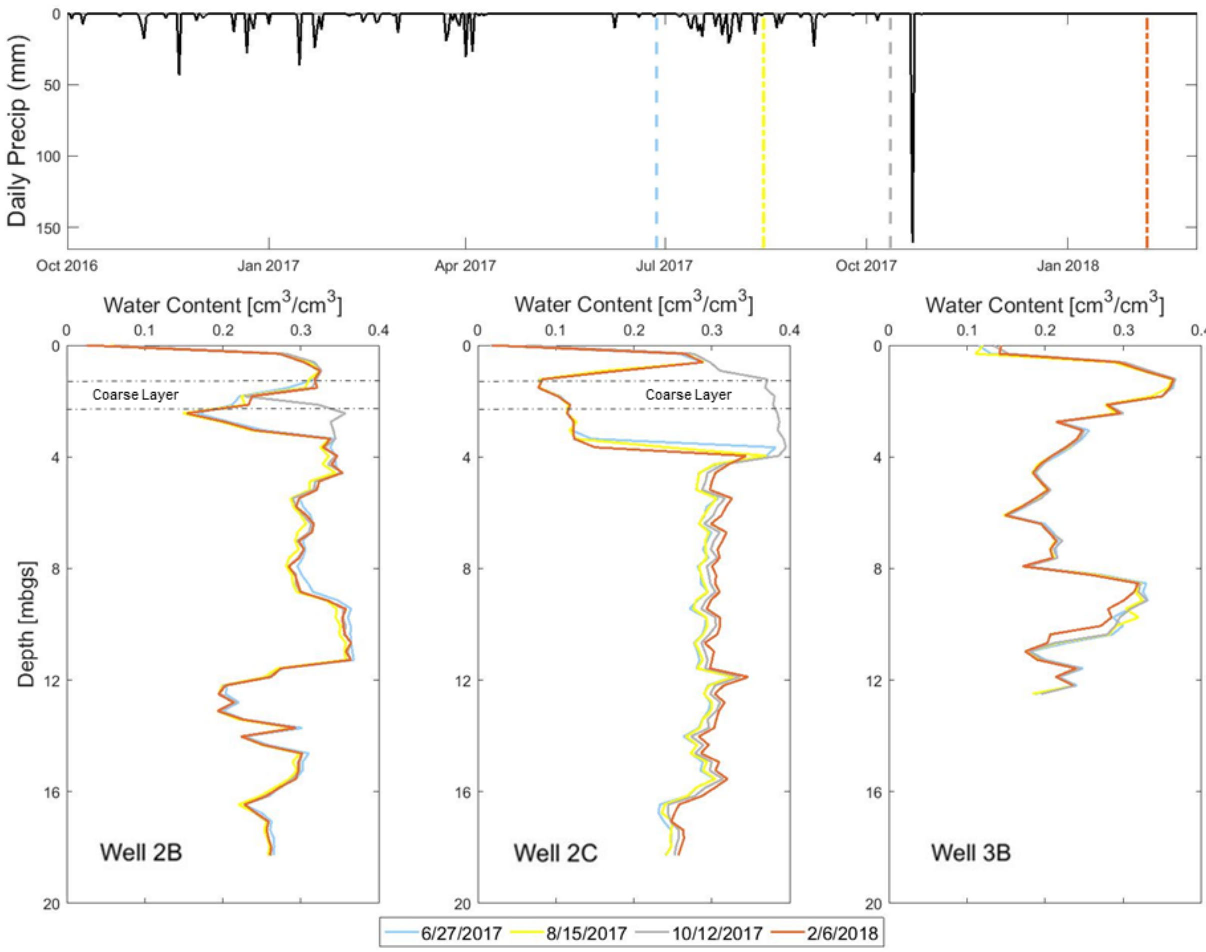

Figure 6: Daily precipitation in mm from Redondo Weather Station above profiles of water content with depth in meters below ground surface for wells 2B, 2C, and 3B. Colors of profiles correspond to timing shown on precipitation figure above. It is important to note that the elevation above sea level of site 2 (3024 masl) and 3 (2989 masl) wells are different. The dotted lines outline the boundary of the coarse gravel-like layer noted in site 2 well logs.

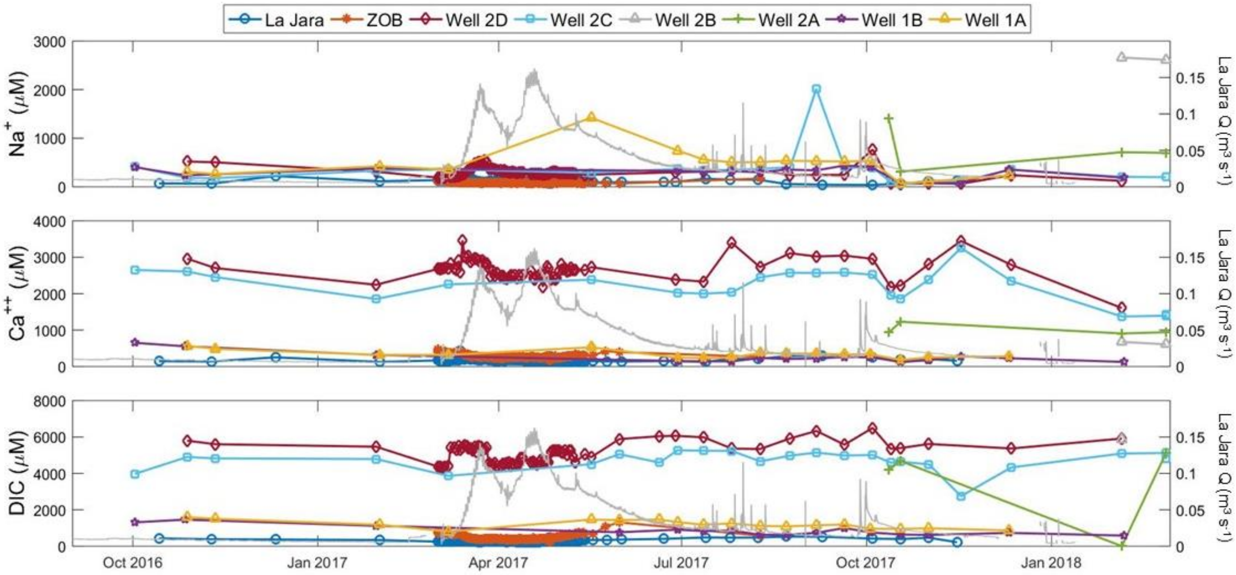

Figure 7: Time series of Na^+, Ca^{2+}, and DIC over WY 2017 for surface waters from La Jara flume and ZOB flume and groundwaters from sites one and two. Concentrations are plotted over La Jara discharge in grey to highlight temporal changes.

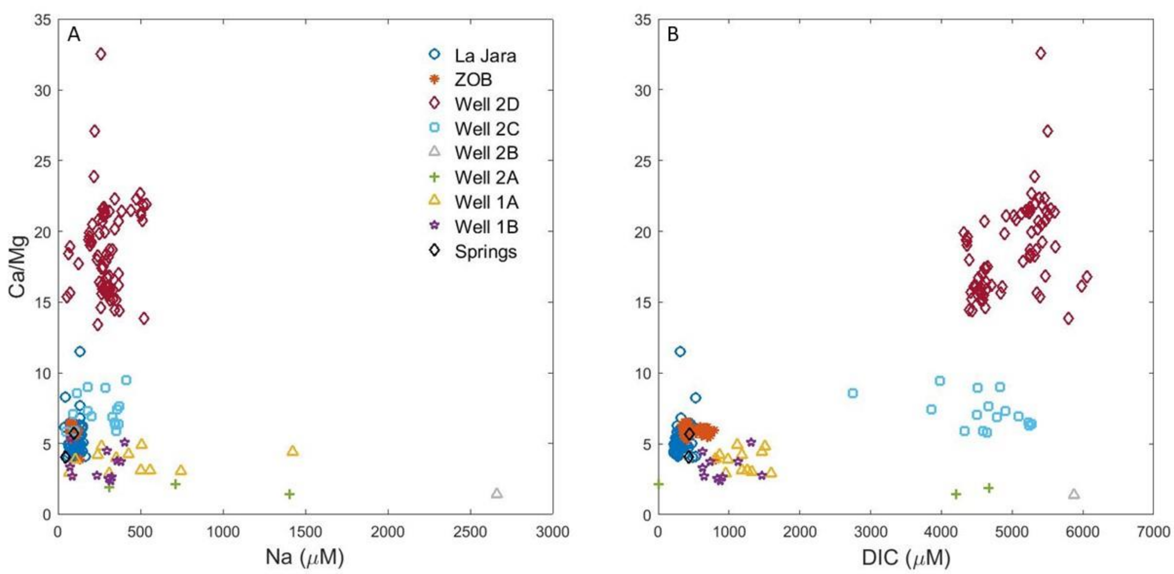

Figure 8: A) Ca^{2+}/Mg^{2+} molar ratios compared to Na^+ concentrations show that groundwater from well 2D have Ca^{2+}/Mg^{2+} ratios that are chemically distinct from the other water stores, which suggest that deeper groundwater is more representative of streamflow than shallow groundwater. B) Ca^{2+}/Mg^{2+} ratios compared to DIC concentrations show that site 1 groundwaters are more representative of contribution to streamflow.

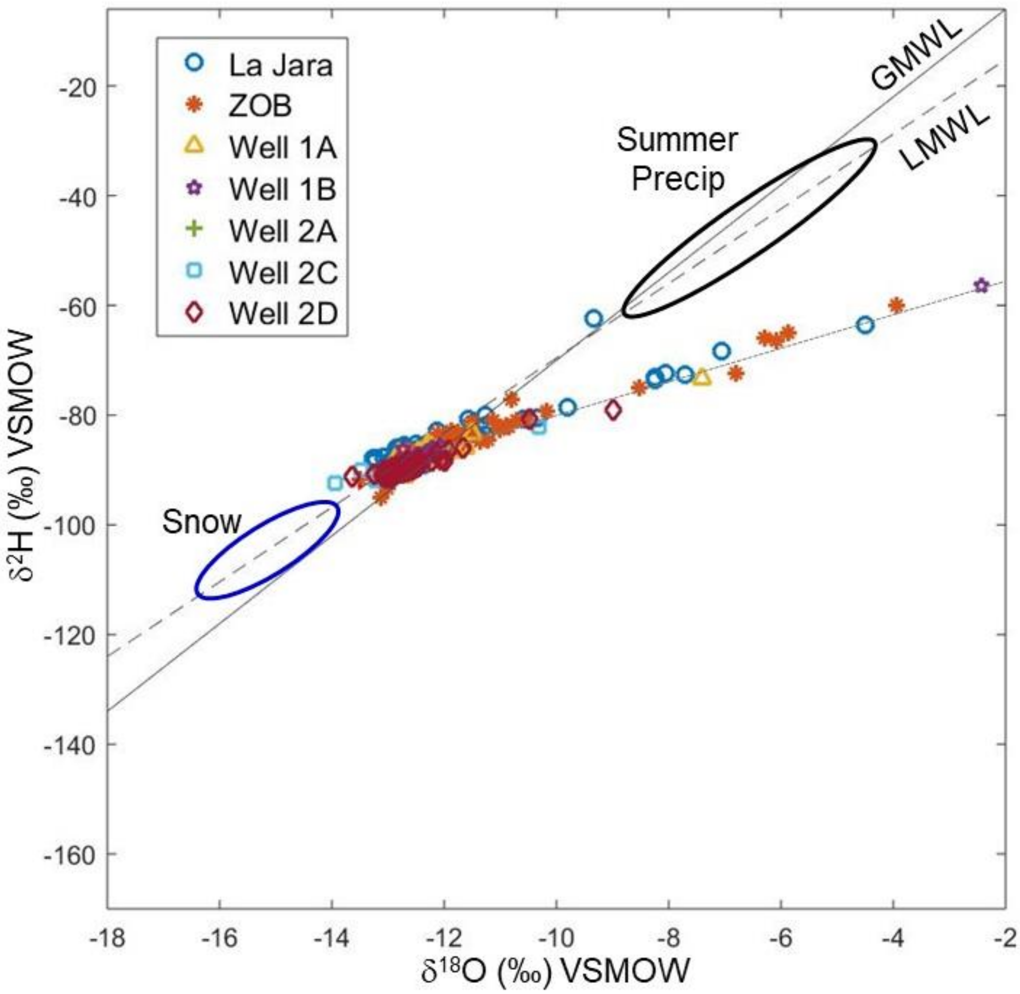

Figure 9: Oxygen ($\delta^{18}O$) and stable hydrogen ($\delta^{2}H$) isotope values of surface waters from La Jara and ZOB flumes, groundwaters, and volume weighted mean ranges of summer precipitation (precip, taken from Zapata-Rios et al., 2015b) and snow (taken from Gustafson, 2008). The global meteoric water line (GMWL, solid line, slope 8.0) and local meteoric water line (LMWL, slope of 6.8, dashed line from Broxton et al., 2009) are plotted for reference. Surface waters and site 1 groundwaters plot along an evaporation trend (dotted line, slope of 3.4).

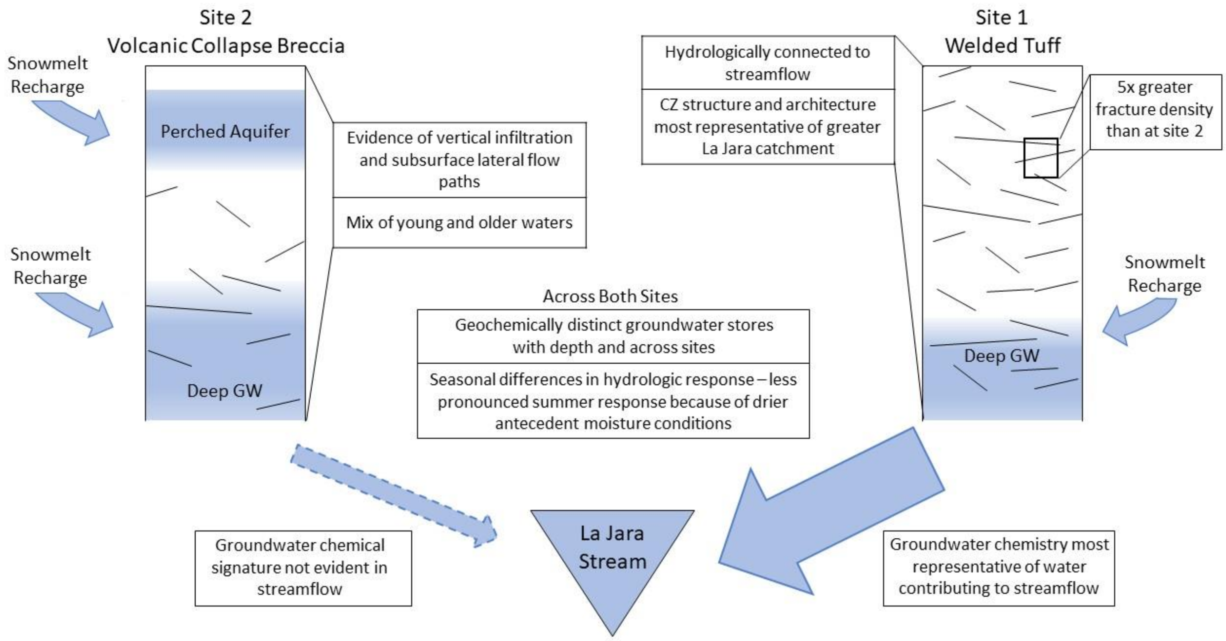

Figure 10. Schematic of intricacies of hydrologic structure and function across two contrasting sites within the ZOB (Sites 1 and 2). Site 2 has multiple, separate stores of groundwater across depth that are distinct from each other and distinct from deep groundwater stores at site 1. All groundwater is recharged via snowmelt and seasonal differences in hydrologic response to precipitation inputs exist at both sites with less pronounced response to summer monsoons. There is evidence of vertical infiltration and subsurface lateral flow at site 2 and a mix of young and older waters, which are expected to persist across all groundwater stores. The fracture density at site 1 is approximately 5 times greater than at site 2 and the CZ structure and architecture of site 1 is most representative of the greater catchment. Deep groundwater from the fractured aquifer system at site 1 is hydrologically connected to streamflow and site 1 deep groundwater chemistry is most representative of water contributing to streamflow while the distinct chemical signature of shallow groundwater from site 2 is not evident in streamflow.

Tables:

Well 2D - Volcanic Collapse Breccia			Well 1A - Welded Tuff		
Date	K_{sat} [m day^{-1}]	Mean K_{sat}	Date	K_{sat} [m day^{-1}]	Mean K_{sat}
6/20/2017	7.46×10^{-3}	7.22×10^{-3}	6/20/2017	1.19×10^{-4}	1.22×10^{-4}
6/28/2017	5.33×10^{-3}		6/29/2017	1.38×10^{-4}	
7/12/2017	8.89×10^{-3}		7/12/2017	1.07×10^{-4}	

Table 1: Estimated saturated hydraulic conductivity in m day^{-1} for three sampling events from wells 2D and 1A and their mean. Estimates were made by curve fitting 15-min VWP data with the KGS model in Aqtesolv.

	n	**Ca^{2+} (µmol/L)**		**Mg^{2+} (µmol/L)**		**Na^{+} (µmol/L)**		**K^{+} (µmol/L)**		**DIC (µmol/L)**		**pH**	
La Jara Flume	160	176.3	*(39.3)*	35.0	*(5.6)*	108.6	*(20.2)*	36.7	*(38.5)*	289.4	*(58.3)*	7.08	(0.37)
ZOB Flume	140	281.3	*(54.9)*	48.1	*(11.8)*	84.8	*(10.1)*	50.3	*(13.3)*	485.9	*(148.0)*	*6.99*	*(0.40)*
Well 1A	18	337.6	*(106.0)*	89.3	*(32.2)*	476.2	*(300.0)*	53.1	*(9.1)*	1198.5	*(225.0)*	7.55	(0.27)
Well 1B	16	254.3	*(144.0)*	72.7	*(39.1)*	286.6	*(117.0)*	57.1	*(22.6)*	851.3	*(250.0)*	7.21	(0.42)
Well 2A	4	1003.0	*(130.0)*	542.6	*(112.0)*	781.6	*(394.0)*	57.2	*(15.1)*	3502.8	*(2046.0)*	7.82	(0.15)
Well 2B	2	643.3	(34.1)	466.0	(15.6)	2636.4	(25.0)	50.2	(3.4)	5870.5	n = 1	8.21	(0.55)
Well 2C	24	2226.0	*(453.0)*	319.1	*(70.5)*	349.8	*(381.0)*	22.8	*(13.4)*	4702.5	*(545.7)*	7.59	(0.18)
Well 2D	84	2663.0	*(283.8)*	146.9	*(22.7)*	298.4	*(110.4)*	44.6	*(12.9)*	5083.1	*(524.8)*	7.51	(0.30)

Table 2: Number of samples (n) and average concentrations of major ions and pH of surface and groundwaters. Standard deviations are shown in italicized parentheses.

		Tritium Analysis						**Radiocarbon Analysis**			
		June 2017			**Feb 2018**			**Feb 2018**			
	Depth to Water (mbgs)	Tritium Content (TU)	Mean Residence Time Piston Flow Model	Mean Residence Time Exponential Model	Tritium Content (TU)	Mean Residence Time Piston Flow Model	Mean Residence Time Exponential Model	$\delta^{13}C_{DIC}$ (‰)	^{14}C (pmC)	Uncorrected ^{14}C age (A_0 = 100 pmC)	Corrected ^{14}C age Mixing Model
Well 2D	2.3 to 3.5	4.1 ± 0.17	13 ± 1.6	20. ± 1.8	4.4 ± 0.27	12 ± 1.8	17 ± 1.7	-13.1	75.34 ± 0.19	2340	621
Well 2C	27.9 to 28.4	1.0 ± 0.19	39 ± 3.7	140 ± 28	0.7 ± 0.18	45 ± 4.8	202 ± 55	-12.4	60.02 ± 0.17	4220	2050
Well 2B	37.6				0.7 ± 0.20	45 ± 5.3	202 ± 60.				
Well 2A	45.1 to 45.7				1.6 ± 0.21	30 ± 2.8	79 ± 12				
Well 1B	35.3 to 38.0	2.0 ± 0.17	26 ± 2.1	59 ± 7.0	2.4 ± 0.24	23 ± 2.3	46 ± 6.0				

Table 3: Tritium content ± lab estimated error and mean residence time calculated with piston flow and exponential models ± age calculation uncertainty of groundwater from wells 2D, 2C, 2B, 2A, and 1B from two low flow sampling events (June 2017 and February 2018). Radiocarbon analysis (pmC of ^{14}C ± lab estimated error and $\delta^{13}C$) of dissolved inorganic carbon from wells 2D and 2C with uncorrected ^{14}C age calculated with A_0 of 100 pmC and corrected.

SUPPLEMENTAL FIGURES AND TABLES

Distinct stores and routing of water in the deep critical zone of a snow dominated volcanic catchment

Alissa White[1], Bryan Moravec[2], Jennifer McIntosh[1], Yaniv Olshansky[2], Ben Paras[1], Andres Sanchez[1], Ty P.A. Ferré[1], Tom Meixner[1], Jon Chorover[2]

[1]Department of Hydrology and Atmospheric Sciences, University of Arizona, Tucson, 85721, USA

[2]Department of Soil, Water, and Environmental Sciences, University of Arizona, Tucson, 85721, USA

Correspondence to: Alissa White (alissawhite@email.arizona.edu)

Well ID	**Well Casing Diameter [cm]**	**Annulus Diameter [cm]**	**Screened Interval Depth [mbgs]**	**Vibrating Wire Piezometer (VWP) or Transducer (T) Depth [mbgs]**	**Total Depth [mbgs]**
1A	2.54	9.6	38.7 to 41.7	VWP @ 41.5	41.7
1B	2.54	9.6	31.7 to 37.8	T @ 37.8	37.8
2A	5.08	9.6	42.8 to 45.9	T @ 45.5	47.15
2B	5.08	9.6	34.7 to 37.8	T @ 37.7	39.1
2C	5.08	9.6	24.7 to 30.8	T @ 30.1	30.85
2D	5.08	9.6	3.7 to 6.7	VWP @ 6.4	6.7
3A	2.54	9.6	13.8 to 16.9	VWP @ 15.3	16.85
3B	5.08	9.6	6.8 to 12.9	VWP @ 12.7	12.93

Supplemental Table 1: Completed well dimensions. All screened intervals are 0.051 cm slotted intervals. It is important to note that VWPs were installed during monitoring well installation while transducers were installed more than one year after drilling; therefore, only VWPs cover the entire time range of this study.

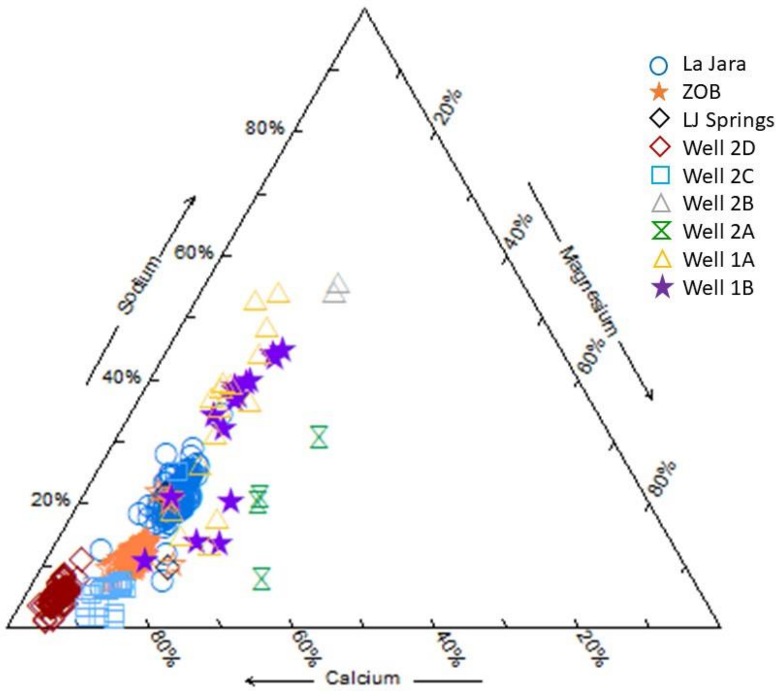

Supplemental Figure 1: Ternary diagram showing percent microequivalents of sodium, calcium, and magnesium. Shallow site two groundwaters are calcium dominant while deeper site two groundwater are more of a mix of calcium-sodium-magnesium and site one groundwaters have a larger range in composition dominated by calcium and sodium. Finally, surface waters from the La Jara flume and La Jara springs are calcium-sodium waters that plot in overlapping space with site one groundwaters and have generally slightly greater percentages of sodium and less percentages of calcium than ZOB surface waters which overlap in space with site one groundwaters and site 2C groundwaters.

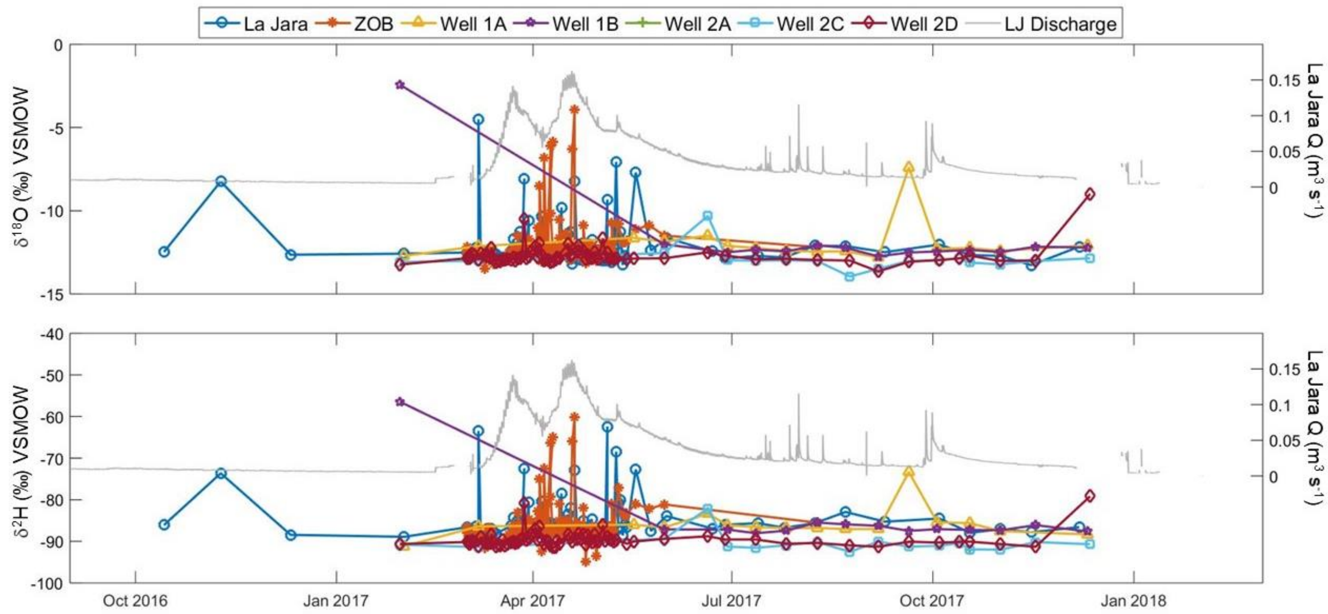

Supplemental Figure 2: Time series of $\delta^{18}O$ and $\delta^{2}H$ surface waters and groundwaters plotted with La Jara discharge to indicate timing of shifts in stable water isotope values.